Ore Geology Reviews 72 (2016) 43–59

Contents lists available at ScienceDirect

Ore Geology Reviews

journal homepage: www.elsevier.com/locate/oregeorev

Geology, geochronology and geochemistry of the Saishitang Cu deposit, East Kunlun Mountains, NW China: Constraints on ore genesis and tectonic setting

Hui Wang [a], Chengyou Feng [a,*], Daxin Li [a], Chao Li [b], Tianzhu Ding [c], Fangzhou Liao [c]

[a] MLR Key Laboratory of Metallogeny and Mineral Assessment, Institute of Mineral Resources, Chinese Academy of Geological Sciences, Beijing 100037, People's Republic of China
[b] National Research Center of Geoanalysis, Beijing 100037, People's Republic of China
[c] Qinghai Saishitang Copper Corporation Ltd., Xining, Qinghai 810003, People's Republic of China

ARTICLE INFO

Article history:
Received 22 March 2015
Received in revised form 1 July 2015
Accepted 6 July 2015
Available online 8 July 2015

Keywords:
Zircon U–Pb
Molybdenite Re–Os
Geochemistry
Ore genesis
Tectonic setting
Saishitang Cu deposit

ABSTRACT

The Saishitang Cu deposit, located on the eastern area of the Eastern Kunlun Orogenic Belt (EKOB), and on the northern margin of the Tibetan Plateau, is one of the most important copper deposits in Qinghai Province, China. Skarn and Cu orebodies mainly occur as stratoids or lenses along the contact zone between the quartz diorite and Lower to Middle Triassic metamorphosed tuff and marble. In this study, we use new zircon U–Pb ages, molybdenite Re–Os ages, granitoid geochemical compositions, and zircon Hf isotope data to constrain the ore genesis and the tectonic setting of the Saishitang Cu deposit. The quartz diorite is composed of inner medium- to fine-grained quartz diorite phase and an outer porphyritic quartz diorite phase. U–Pb dating of zircons by laser ablation–inductively coupled plasma–mass spectrometry (LA–ICP–MS) yield ages of 222.7 ± 2.3 Ma and 222.6 ± 2.4 Ma for the inner and outer phase of quartz diorite, respectively. Molybdenite separated from ore-bearing quartz veins yields a Re–Os isochron age of 223.4 ± 1.5 Ma, indicating a close temporal link between magmatism and mineralization. Geochemically, the quartz diorite shows high contents of SiO_2 (59.63–68.21 wt.%), Al_2O_3 (15.57–18.13 wt.%) and Na_2O (3.07–3.56 wt.%), with A/CNK values between 0.90 and 1.01 and Mg# between 46 and 52, classified as the calc-alkaline I-type granite. The trace element patterns are characterized by high LREE (LREE/HREE = 7.36–13.03), weak negative Eu anomalies (δEu = 0.69–0.86), relative enrichment of Rb, Th, K, and Pb, and depletion of Nb, Ta, P, and Ti. The quartz diorite has variable $\varepsilon_{Hf}(t)$ values (−2.5 to 4.87) and Mesoproterozoic two-stage model ages (997 to 1387 Ma). Based on petrological and geochemical features, we infer that the quartz diorite is derived from the partial melting of thickened lower crust with an additional input of mantle components. According to the geological, geochemical, and mineralogical features, we propose that the Saishitang Cu deposit is a skarn deposit with minor porphyry-type mineralization and the porphyry–skarn mineral system is related to the crust–mantle interaction. Based on the tectonic evolution of the Paleo-Tethys Ocean during the Late Triassic, we infer that the intrusions and associated Cu mineralization were related to regional extension of the EKOB in a post-collision environment. The results also show that most porphyry–skarn Cu deposits in the EKOB have similar mineralization ages (240–220 Ma) and the Late Triassic granitoids in the EKOB present significant potential for the prospecting of porphyry–skarn Cu deposits.

1. Introduction

The Eastern Kunlun Orogenic Belt (EKOB), which is located in the northern part of the Qinghai–Tibetan Plateau, includes (from west to east) the Qimantagh Mountains, the Buerhanbuda Mountains, and the Ela Mountains. The EKOB, as a constituent part of the Tethys metallogenic belt, represents the most important region of Triassic deposits in China (Mao et al., 2012). Recently, many large- or medium-sized porphyry–skarn Cu–polymetallic deposits have been found and studied in the EKOB, including the Kaerqueka, Hutouya, Yaziou, Wulanwuzhuer, and Tuoketuo deposits (She et al., 2007; Li et al., 2008, 2011; Feng et al., 2011; Xia et al., 2014a). However, the porphyry–skarn mineral system of EKOB remains poorly understood. Although most porphyry–skarn copper systems are found in subduction-related environment (Cooke et al., 2005; Mao et al., 2014), many porphyry deposits are also present in collisional zones or intracontinental settings which have been identified and studied in recent years (Hou et al., 2013; Zhou et al., 2015; Pirajno and Zhou, 2015). It is noted that, in the Tethys metallogenic belt, numerous porphyry, epithermal and skarn deposits postdating the closure of oceanic subduction have been documented (e.g., the Sari Gunay epithermal Au deposit in Iran,

* Corresponding author.
E-mail address: fengchy@cags.ac.cn (C. Feng).

http://dx.doi.org/10.1016/j.oregeorev.2015.07.002
0169-1368/

Richards, 2009; the Gangdese porphyry–skarn Cu belt in Tibet, Hou et al., 2013; the Yangla skarn deposit in Yunnan, Zhu et al., 2015).

The Ela Mountains, the most easterly part of the EKOB, have a complex geological history that records episodes of both sedimentation and magmatic activity related to different tectonic environments (e.g., especially from 260 to 200 Ma; Yin et al., 2004; Zhang et al., 2004a; Li et al., 2014). The Saishitang Cu deposit is a medium-sized deposit located in the southeast part of the Ela Mountains. The deposit was first identified in 1955 and has been the subject of significant exploration and study. However, as a result of extensive exploitation, it now faces significant resource depletion. Previous studies have proposed different theories regarding the genesis of the Saishitang deposit, including skarn-type (QGT, 1983; Xin et al., 2013; Cheng et al., 2014; Wang et al., 2015), exhalative sedimentary-type (Li et al., 1993; Song et al., 1995), and porphyry-type (Li et al., 2009a; Wu, 2010; Wei et al., 2012). The isotopic ages of intermediate-felsic intrusions are 205.7–248 Ma (Li et al., 2009a; Liu et al., 2012a), but no precise age has been reported for the metallogenesis. Limited geochronological and geochemical data indicate that the intrusions of the Saishitang deposit were formed in an active continental margin (Lai et al., 2010) or in an intracontinental orogeny setting (Liu et al., 2012a).

Recent exploration and mining exposures at the Saishitang Cu deposit have made detailed investigation and research possible. This study reports new zircon U–Pb dating, molybdenite Re–Os dating, granitoid geochemical data, and zircon Hf isotope data, and discusses the geochronology, petrogenesis and ore genesis. Furthermore, our new data may provide strong constrains on the geodynamic setting of the intrusions and associated Cu mineralization in the Saishitang Cu deposit.

2. Geological background

The EKOB has documented a complicated history of seafloor spreading, subduction, and collision between Bayan Har terrane and the EKOB since the Early Paleozoic (Jiang et al., 1992; Yang et al., 1996; Yin and Harrison, 2000). It is bound to the north by the Qaidam Basin, to the south by the Bayan Har Orogenic Belt, to the east by the West Qinling Orogenic Belt (WQOB), and to the west by the NE-trending Altyn Fault (Fig. 1a, b). The EKOB consists of three tectonic units, the Northern, Middle and Southern Zones, separated by major faults (Fig. 1c; Jiang et al., 1992). The A'nyemaqen suture zone along the southern margin of the EKOB records the closure of the Paleo-Tethys Ocean and a continental collision event (Yang et al., 1996). The A'nyemaqen Ocean is an important branch of the Paleo-Tethys Ocean, which is supported by the Haerguole ophiolites (LA–ICP–MS U–Pb age of zircons from gabbros, 332.8 ± 3.1 Ma; Liu et al., 2011) and the Derni ophiolites (whole rock ^{40}Ar–^{39}Ar age of basalts, 345.3 ± 7.9 Ma; SHRIMP U–Pb age of zircons from basalts, 308.2 ± 4.9 Ma; Yang et al., 2004). These data show that the A'nyemaqen Ocean probably has opened at least as early as 308 Ma. Although the timing of closing of the Ocean and continental collision remains controversial, there is a growing consensus that the

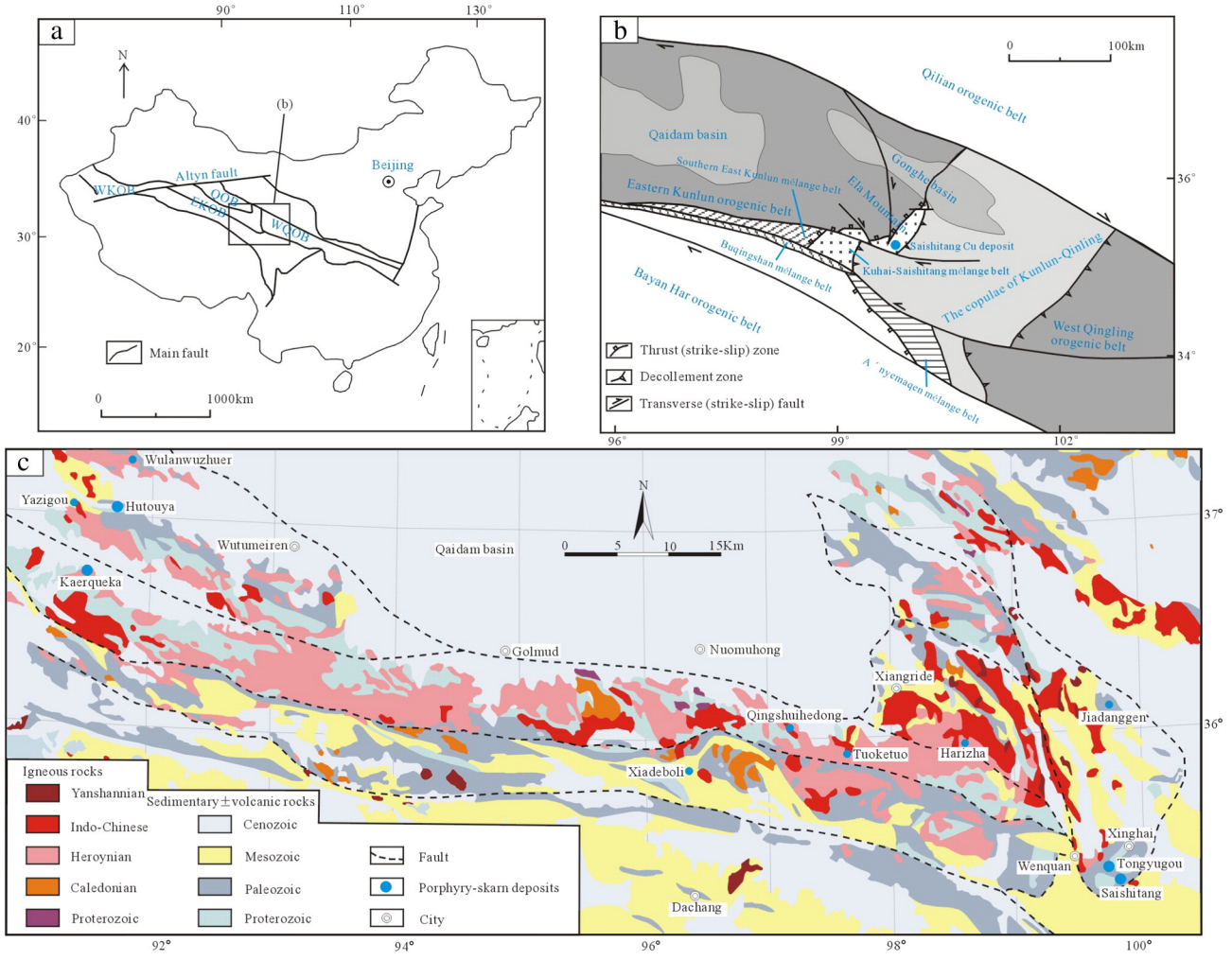

Fig. 1. (a) Schematic map showing the major tectonic units of the western Central Orogenic Belt (COB) of China, including the West Kunlun Orogenic Belt (WKOB), the East Kunlun Orogenic Belt (EKOB), the Qilian Orogenic Belt (QOB), and the West Qinling Orogenic Belt (WQOB). (b) Schematic map showing the location of the Saishitang Cu deposit and adjacent tectonic units (after Zhang et al., 2004b). (c) Schematic geological map showing the distribution of granitoids in the EKOB (modified after Xia et al., 2015).

collision was ended at about 230 Ma, and in the Late Triassic to Early Jurassic (230–190 Ma), the Eastern Kunlun area went into the intracontinental orogenic stage (Guo et al., 1998; Mo et al., 2007; Zhang et al., 2012; Xia et al., 2015; Hu et al., 2015).

The basement beneath the EKOB is composed of the Paleo- and Mesoproterozoic Kuhai Group, Jinshuikou Group (zircon U–Pb ages of 1270–1486 Ma; Lu et al., 2009), Wanbaogou Group (zircon U–Pb ages of 1343 ± 30 Ma; Wang et al., 2007) and Neoproterozoic Binggou Group. The Paleozoic rocks consist of the Late Ordovician to Early Carboniferous marine sediments (including Tanjianshan Group and Maoniushan Formation). It is noted that there are two important angular unconformities within the Late Paleozoic to Early Mesozoic sequences. One is between the Upper Permian Gequ Formation and the underlying Upper Carboniferous Haoteluowa Formation, and the other lies between the Upper Triassic Elashan (Babaoshan) Formation and the underlying Lower to Middle Triassic Hongshuichuan Formation. The former was considered as a continental uplift event in response to the collision between the Bayan Har terrane and the EKOB (Jiang et al., 1992). However, the latest studies suggest the latter marks the collision event, whereas the former represents the initiation of northward subduction of the Hohxil–Songpan–Ganzi Ocean (Liu, 2011a; Li et al., 2012a, 2015).

The plutonic rocks in The EKOB include Ordovician–Silurian and Permian–Triassic units (Fig. 1c; Pan et al., 2004; Chen et al., 2012). The Permian–Triassic granitoids are dominant in the EKOB with an area of 23,000 km^2 (Liu et al., 2004). The Late Permian to Middle Triassic igneous rocks of the EKOB are considered to be the product of the northward subduction of the A'nyemaqen Ocean (Zhang et al., 2012; Li et al., 2013; Wang et al., 2014), while the Late Triassic granitoids are thought to have been generated during the post-collision orogenic stage (Zhang et al., 2006; Feng et al., 2012; Li et al, 2012a; Wang et al., 2014; Luo et al., 2014).

The Saishitang Cu deposit is located in southeastern Ela Mountains, the easternmost region of the EKOB, and occurs within the Kuhai–Saishitang mélange belt, which is connected with the A'nyemaqen and Buqingshan mélange belts to the south (Fig. 1b). The majority of regional strata is non-Smithian (Zhang et al., 2014a) and consists of tectonic slices of different ages and genesis, including a crystalline basement complex of a Proterozoic orogeny, an Early to Middle Triassic flysch formation, clastic–volcanic–carbonate rock formations, and Late Triassic terrestrial volcanic rocks (Elashan Formation). An orogeny accompanied by multi-level thrusting led to the different stratigraphic units being superimposed on each other, and produced folds and faults that mainly strike to the W and NW–NNW. Granitoids in the Ela Mountain area, which formed mainly during the Middle to Late Triassic period, extend along a NW–NNW orientation and are composed mainly of quartz diorite and granodiorite. In addition to the Saishitang Cu deposit, other Cu–polymetallic deposits in this area include the Touyugou, Rilonggou, Jiadanggen, and Suolaigou deposits.

3. Ore deposit geology

The Saishitang Cu deposit is situated ~60 km southwest of Xinghai County, Qinghai Province (E99°35′–E99°50′, N35°15′–N35°25′), at an altitude of 3600–4000 m. The deposit is currently mined by West Mining Co. Ltd. of China, with total copper metal reserves estimated to be 374,000 t (Gu et al., 2012).

The mining area consists mainly of Middle–Lower Triassic, Paleogene–Neogene, and Quaternary lithologies as well as a slice of Proterozoic high-grade metamorphosed rocks. The Middle–Lower Triassic units are sedimentary–volcanic rocks that underwent extensive contact metamorphism. They can be divided into four sections according to their lithological association and rhythmic bedding (Fig. 2). Skarn and orebodies occur mainly in the contact between intrusions and the third lithological section, which consists of metamorphosed tuff and marble containing metamorphosed siltstone (Fig. 3). The volcanic rocks of this third section are mainly metamorphosed andesitic–dacitic crystal tuff intercalated with andesite. The main tectonic structure is oriented NW and is dominated by folds. The Xueqinggou complex fold is situated in the eastern part of the mining area and trends NW. The Saishitang anticline is a secondary fold, located on the southwestern limb of the Xueqinggou fold, which controls the stratigraphic distribution in the mining area (Fig. 2). As a result of the lithological differences, the formation of folds has resulted in extensive interlayer gliding and delamination structures, which provide favorable spaces for hydrothermal flow and the precipitation of ore minerals. Zhang et al. (2014b) identified four stages of folding (F_1 to F_4) and considered that the emplacement of the intrusions occurred between F_1 and F_2. Several small-scale NW–NNW and W trending faults also occur within the mining area.

The intrusive units intruded the core of the Saishitang anticline as a NW–SE oriented stock, with an outcrop area of ca. 3 km^2 (Fig. 2). Based on cross-cutting relationship and petrographic characteristics, two stages of magmatism have been recognized. The quartz diorite complex intruded in the early stage, composed of an inner medium- to fine-grained quartz diorite phase and an outer porphyritic quartz diorite phase, with quartz diorite porphyry and diorite porphyry as dykes, while granite porphyry, granodiorite porphyry and rhyolite porphyry were formed later as small dykes or stocks. The medium- to fine-grained quartz diorite (Fig. 4a, c) is composed of plagioclase (50%–55% by volume), K-feldspar (5%–10%), quartz (15%–20%), biotite (10%–15%), and hornblende (5%–10%), together with accessory apatite, zircon, titanite, and ilmenite. The pophyritic quartz diorite is medium- to fine-grained, contains more quartz (mainly fine-grained matrix quartz) than medium- to fine-grained quartz diorite, and shows a clear porphyritic texture (Fig. 4b, d). The quartz diorite complex is spatially associated with the skarn and mineralization (Fig. 2), which is considered as the causative intrusion (Li et al., 2009a; Xin et al., 2013).

In total, 116 copper orebodies, 32 lead–zinc orebodies, and 2 iron orebodies have been identified within the mining area. The main orebodies mainly occur in the contact between metamorphosed tuff and marble and there are also some non-economic orebodies (considered as porphyry-type) which occurred within the intrusions, such as porphyritic quartz diorite, diorite porphyry and granite porphyry. The main orebodies are stratoid, lenticular, and veined, and are generally NW-trending and SW dipping (at 20°–40°; Fig. 3). The orebodies are controlled mainly by the stratigraphic lithological contacts and they are relatively discontinuous and irregular (Xin et al., 2013). The ores are closely associated with skarn and include pyrrhotite–chalcopyrite, pyrite–chalcopyrite, and magnetite–chalcopyrite types. The ore structures are mainly massive and disseminated, followed by stockwork and banded. Ore minerals are mainly chalcopyrite, pyrrhotite, pyrite, and magnetite, followed by sphalerite, galena, stannite, arsenopyrite, and a small amount of bornite, molybdenite, and chalcocite.

The alteration and mineralization of the Saishitang deposit are mainly developed in the contact zone between quartz diorite and wall rocks. The main hydrothermal alteration type includes skarnization, silicification, chloritization and carbonation, with minor potassic alteration. Skarn alteration mainly occurs in the exocontact zone, producing calc-silicates including prograde and retrograde skarns. Silicification, chloritization and carbonation are widespread distribution in both intrusions and wall rocks. The inner contact zone is relatively narrow and the endoskarn consists mainly of diopside with quartz, sericite, chlorite and disseminated or veined chalcopyrite and pyrite. From quartz diorite to the wall rocks, different alteration zones were identified, including a potassic alteration zone, a phyllic zone, a skarnization zone and a propylitization zone (Li et al., 2009a).

Field and textural relationships indicate the skarn- and ore-forming processes can be divided into four stages: (I) a prograde skarn stage; (II) a retrograde skarn stage; (III) a quartz–sulfide stage; and (IV) a quartz–carbonate stage (Wang et al., 2015). The prograde skarn stage

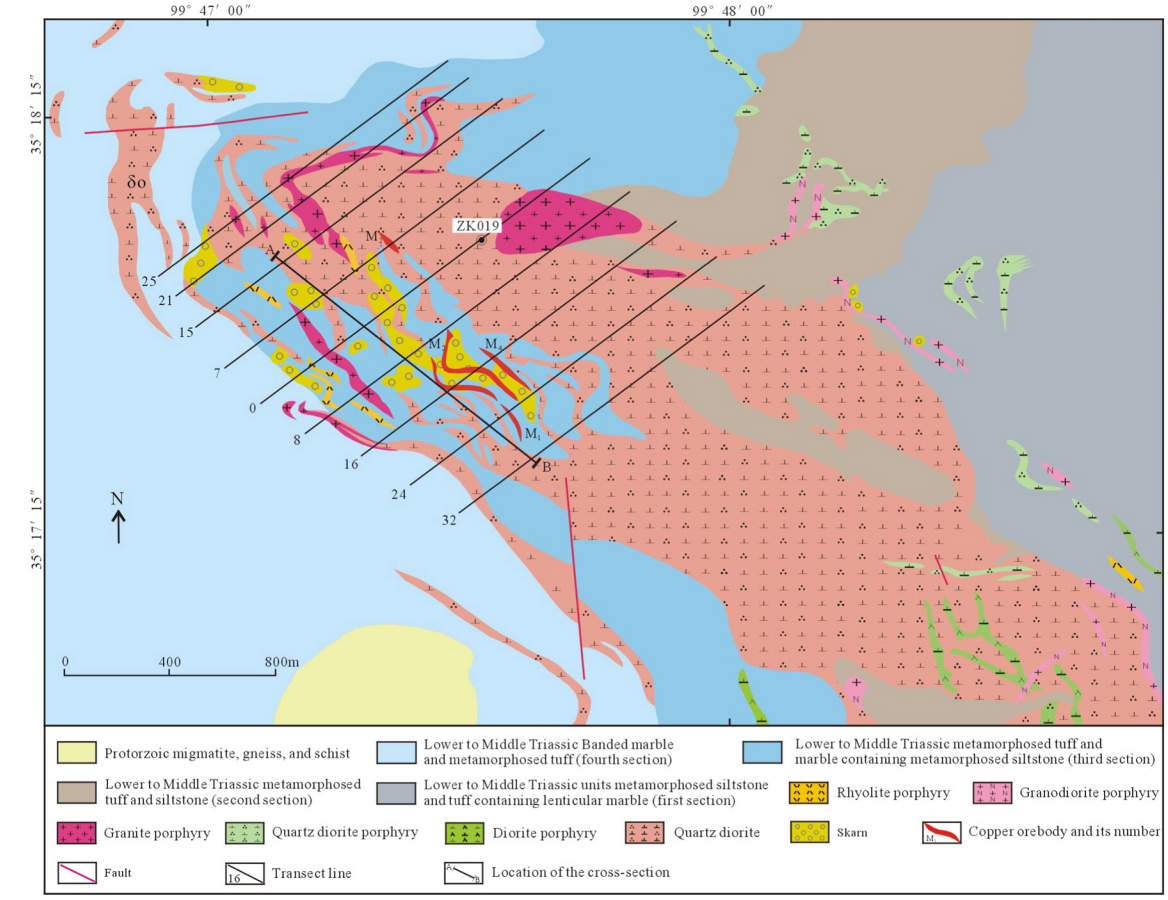

Fig. 2. Geological map of the Saishitang Cu deposit, Qinghai Province, China (modified from Li et al., 2012b).

(I) is characterized by the formation of abundant garnet, pyroxene and wollastonite, and minor magnetite. The garnet is dominantly grossular, with minor andradite, while the pyroxene is diopside and hedenbergite. Wollastonite occurs mainly in the contact between the intrusions and the marble. The garnet–pyroxene skarn is mostly massive (Fig. 5a), although there are also some banded skarns, most of which contain

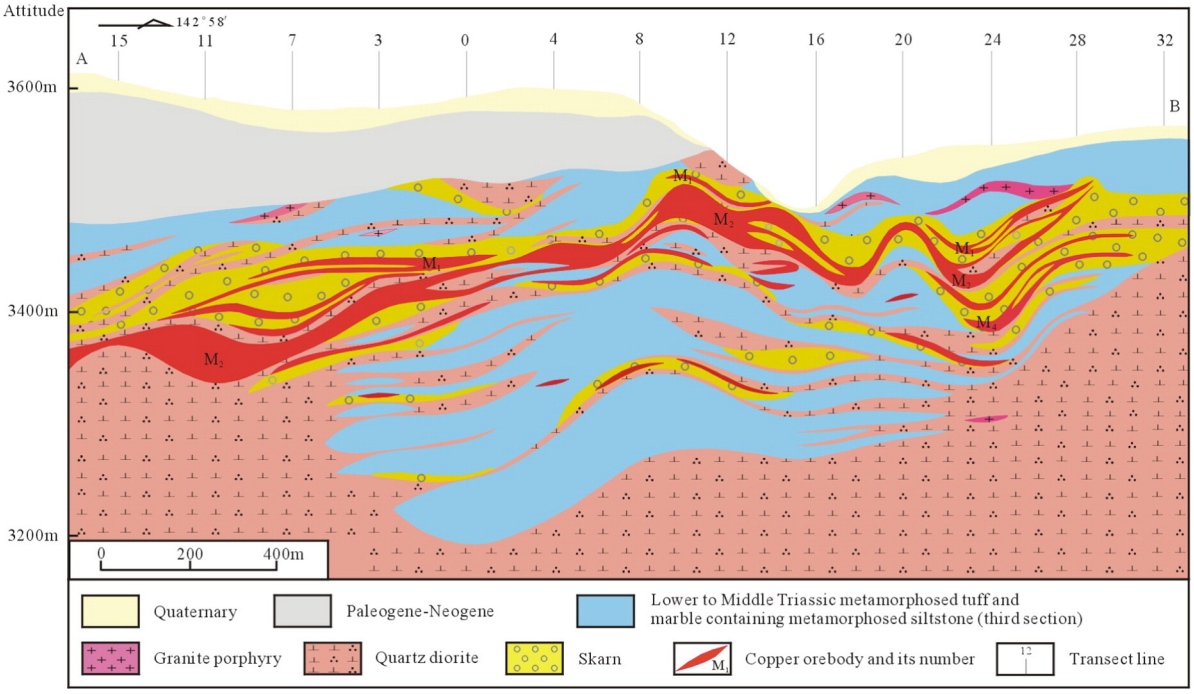

Fig. 3. Geological cross-section (A–B) through the Saishitang Cu deposit (as shown in Fig. 2).

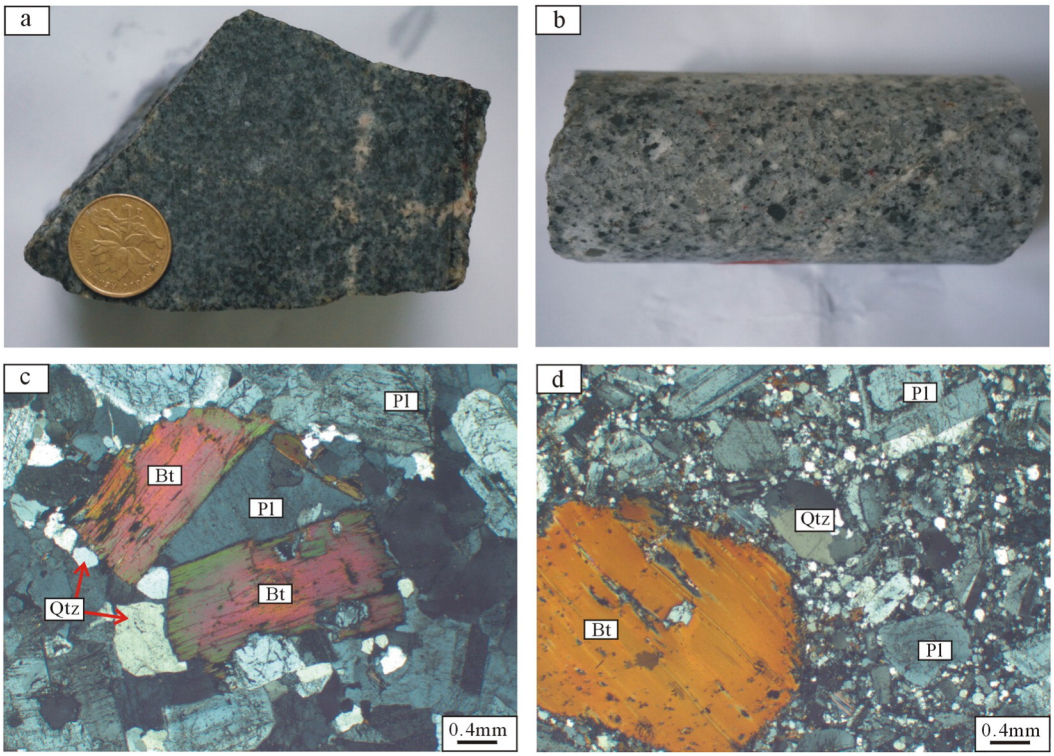

Fig. 4. Hand specimen photographs (a, b) and thin section photomicrographs (c, d; cross-polarized light) of medium- to fine-grained quartz diorite and porphyritic quartz diorite of the Saishitang Cu deposit. Abbreviations: Bt = biotite; Pl = plagioclase; Qtz = quartz.

skarn veins that cut across sedimentary beds and that crystallized nearly contemporaneously in all cases (Fig. 5b). The retrograde skarn stage (II) is marked by the formation of a magnetite–amphibole assemblage (Fig. 5c), with large amounts of epidote, which replaced the garnet and pyroxene. The quartz–sulfide stage (III) is characterized by the precipitation of large amounts of sulfides (e.g., chalcopyrite, pyrrhotite, and pyrite) along with gangue minerals (e.g., quartz, chlorite, and sericite), and represents the main ore-forming stage. The quartz–carbonate stage (IV) mainly produced quartz–carbonate veins, but is also associated with lesser chalcopyrite, pyrite, and sphalerite. Chalcopyrite is closely associated with the skarn (Fig. 5d, e), while pyrrhotite and molybdenite were replaced by chalcopyrite (Fig. 5f, g). The paragenesis of molybdenite and chalcopyrite suggests that they precipitated in the same stage. Hence, molybdenite Re–Os dating can be used to determine the timing of chalcopyrite formation. Stannite, which was precipitated during early stage III, replaced sphalerite (Fig. 5 h).

4. Sample preparation and analytical methods

4.1. Sample preparation

A medium- to fine-grained quartz diorite sample (ST05) was chosen from outcrops at the surface of the mining area (N35°17.604′, E99°48.022′) for zircon U–Pb dating and in situ Hf isotopic analysis, and a porphyritic quartz diorite sample (ZK2523B-02) was collected from ~200 m depth in the drill core ZK2523B-02 (underground drilling in the No. 23 prospecting line at the 3250 level) for zircon U–Pb dating. Five molybdenite samples, collected at 65–150 m depth in drill core ZK019 (Fig. 2), were selected for Re–Os isotopic dating. Molybdenite was identified in quartz veins or as disseminated in the skarn-type ores and coexisting with chalcopyrite (Fig. 5f). Six medium- to fine-grained quartz diorite samples (ST05, ST06 ST07, ST09-1, ST09-2 and ST09-3) and two porphyritic quartz diorite samples (2021B03-18 and 2021B03-19, collected at depths of 123 m and 126 m, respectively, in drill core ZK2021B-03, underground drilling in the No. 21 prospecting line at the 3220 level) were sampled for major and trace element analyses.

4.2. Analytical methods

4.2.1. Zircon U–Pb dating

Zircons were separated from each ~3 kg sample using standard density and magnetic separation techniques. Zircon grains were handpicked and mounted in an epoxy resin disk, and then polished and coated with gold. Before analysis, the sample surface was cleaned with ethanol to eliminate possible contamination. All zircons were photographed in transmitted and reflected light, and imaged with cathodoluminescence (CL) to identify suitable crystals and locations for U–Pb analyses. Zircon U–Pb dating was performed using laser ablation inductively coupled plasma mass spectrometry (LA–ICP–MS) at the Institute of Geology and Geophysics, Chinese Academy of Sciences, Beijing, China. An Agilent 7500a quadruple (Q) ICP–mass spectrometer with a 193 nm excimer ArF laser-ablation system (GeoLas Plus) were used for the determination of zircon U–Pb ages. After the analysis of every 10 samples, measurements of two standards were made, the Harvard zircon 91500 and GJ-1. Zircon 91500 was used as external standard to correct instrumental mass discrimination and elemental fractionation and zircon GJ-1 was used for quality control. A mean age of 1064 Ma was obtained for the 91500 zircon standard. Data were collected using a 35 μm diameter beam. Detailed operating conditions and data reduction methodology are as described by Xie et al. (2008). The $^{207}Pb/^{206}Pb$ and $^{206}Pb/^{238}U$ ratios were calculated using GLITTER 4.0 (Griffin et al., 2008). Common Pb was corrected following Anderson (2002). The weighted mean U–Pb ages and concordia plots were processed using ISOPLOT 3.0 (Ludwig, 2003).

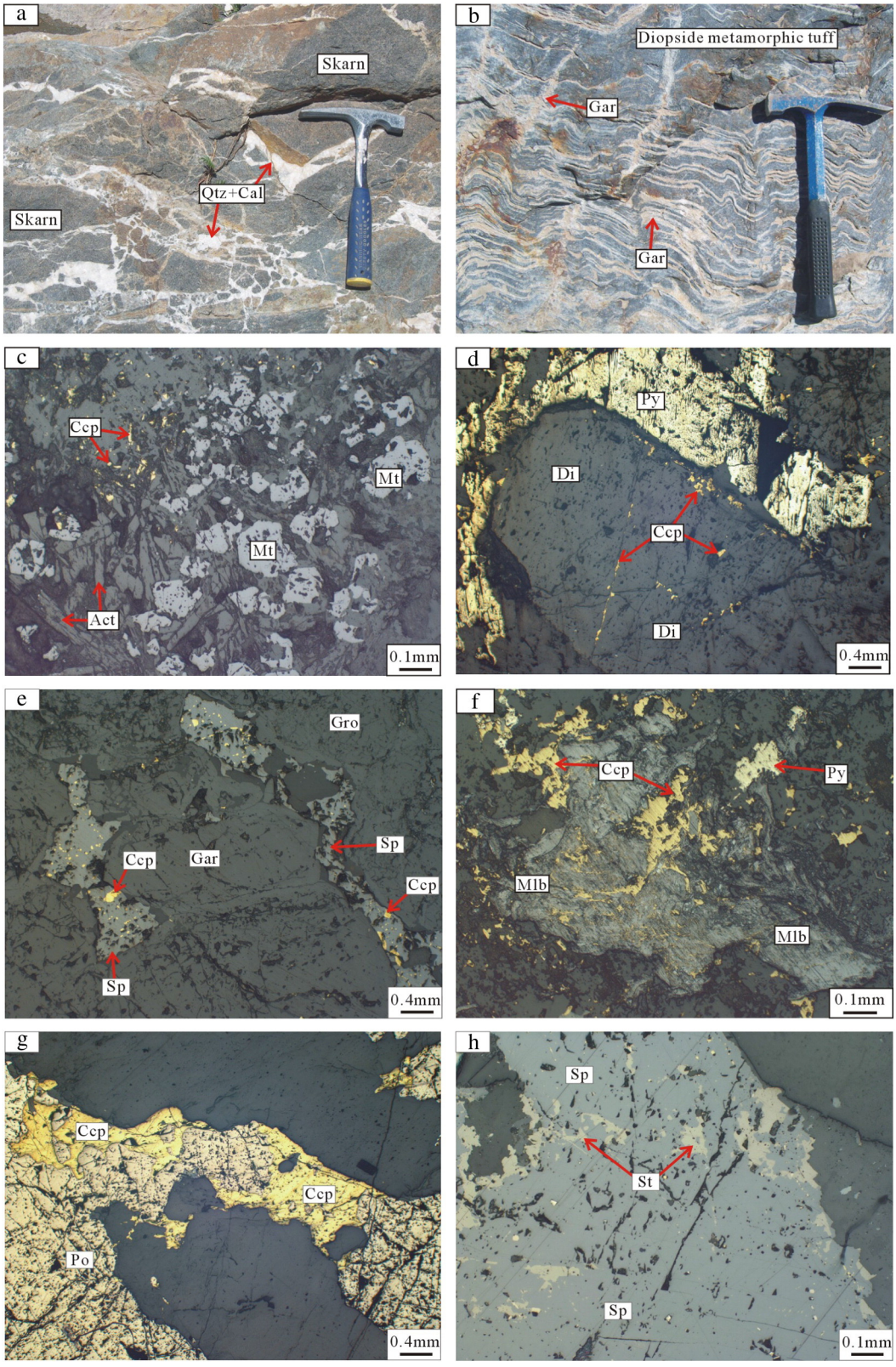

Fig. 5. Photographs of skarn and mineralization features in the Saishitang Cu deposit. (a) Massive skarn cut by a quartz–calcite vein. (b) Diopside metamorphosed tuff with garnet band. (c) Granular magnetite and disseminated chalcopyrite in actinolite skarn (reflected light). (d) Chalcopyrite and pyrite replacement of coarse-grained diopside. (e) Sphalerite vein with droplet-like chalcopyrite in garnet skarn (reflected light). (f) Molybdenite replaced by chalcopyrite (reflected light). (g) Pyrrhotite replaced by chalcopyrite (reflected light). (h) Sphalerite replaced by stannite (reflected light). Abbreviations: Act = actinolite; Bn = bornite; Cal = calcite; Ccp = chalcopyrite; Di = diopside; Gar = garnet; Mlt = molybdenite; Mt = magnetite; Po = pyrrhotite; Py = pyrite; Qtz = quartz; Sp = Sphalerite; St = stannite.

4.2.2. Molybdenite Re–Os dating

A heavy liquid separation method was first applied to separate molybdenite from the finely crushed (80–100 mesh) rocks. Second, molybdenite grains were handpicked individually under a binocular microscope to ensure molybdenite separates of >99% purity. Finally, Re–Os isotope analysis was performed at the National Research Center of Geoanalysis (NRCG), Chinese Academy of Geological Sciences, Beijing, China. Samples were dissolved and equilibrated with ^{185}Re- and ^{190}Os-enriched spikes using alkaline fusion. The separation of rhenium from matrix elements was achieved by solvent extraction and cation exchange resin chromatography, while osmium was distilled as OsO_4 from an H_2SO_4–$Ce(SO_4)_2$ solution. All isotopic measurements were made by ICP–MS (VG Plasma Quad). For details of the chemical procedures, see Shirey and Walker (1995) and Du et al. (2004). The modal age (t) was calculated as follows: $t = [\ln(1 + {}^{187}Os/{}^{187}Re)] / \lambda$, where λ (^{187}Re decay constant) $= 1.666 \times 10^{-11}$/a (Smoliar et al., 1996). The blanks in this experiment were 0.0035 ng for rhenium and 0.00021 ng for ^{187}Os. Data were processed by calculating isochronal and weighted mean ages, and preparing concordia diagrams using the Isoplot software (Ludwig, 2003).

4.2.3. Major and trace element analyses

Following the removal of weathered surfaces, the samples were crushed and then ground to 200 mesh using an agate mill. Major and trace element analyses were performed at the NRCG, Chinese Academy of Geology Sciences, Beijing, China. Major element data were collected using a 3080E X-ray fluorescence spectrometer with a relative standard deviation (RSD) of <2%–8%, with FeO analyzed by the titration method (RSD = 10%). Loss on ignition (LOI), calculated as the weight difference between burning and very high-temperature (1000 °C) heating, had an RSD of <5%. Trace element and REE abundances were determined by ICP–MS (X-series). The analytical uncertainties for major elements were generally within 1%–5%, while the in-run analytical precision for most trace elements was better than 5%.

4.2.4. Hf isotopic analyses

In situ Hf isotopic analyses were performed on the same zircon grains preciously analyzed for U–Pb, using a Neptune MC–ICP–MS coupled to a GeoLas UP193 laser ablation microprobe with a beam size of 44 μm and a laser pulse frequency of 8–10 Hz at the State Key Laboratory of Continental Tectonics and Dynamics, Chinese Academy of Geological Sciences. During the analysis, He was used as the carrier gas. International standard zircon samples GJ-1 were used as reference. Details of instrumental conditions and test process were given in Wu et al. (2006). The initial $^{176}Hf/^{177}Hf$ ratios and $\varepsilon_{Hf}(t)$ values were calculated with reference to the chondritic reservoir (CHUR) at the time of zircon growth from magmas. The decay constant for ^{176}Lu of 1.867×10^{-11} year^{-1} (Soderlund et al., 2004), and the chondritic $^{176}Hf/^{177}Hf$ ratio of 0.282772 and $^{176}Lu/^{177}Hf$ ratio of 0.0332 (Blichert-Toft and Albarède, 1997) were adopted. The depleted mantle model ages (T_{DM}) used for basic rocks were calculated with reference to the depleted mantle at the present-day $^{176}Hf/^{177}Hf$ ratio of 0.28325, similar to that of the average mid-ocean ridge basalt (MORB) (Nowell et al., 1998) and $^{176}Lu/^{177}Hf = 0.0384$ (Griffin et al., 2000). Zircon Hf isotopic crustal model ages (T_{GM}^{C}) were calculated using an average continental crustal $^{176}Lu/^{177}Hf$ ratio of 0.015 (Griffin et al., 2002).

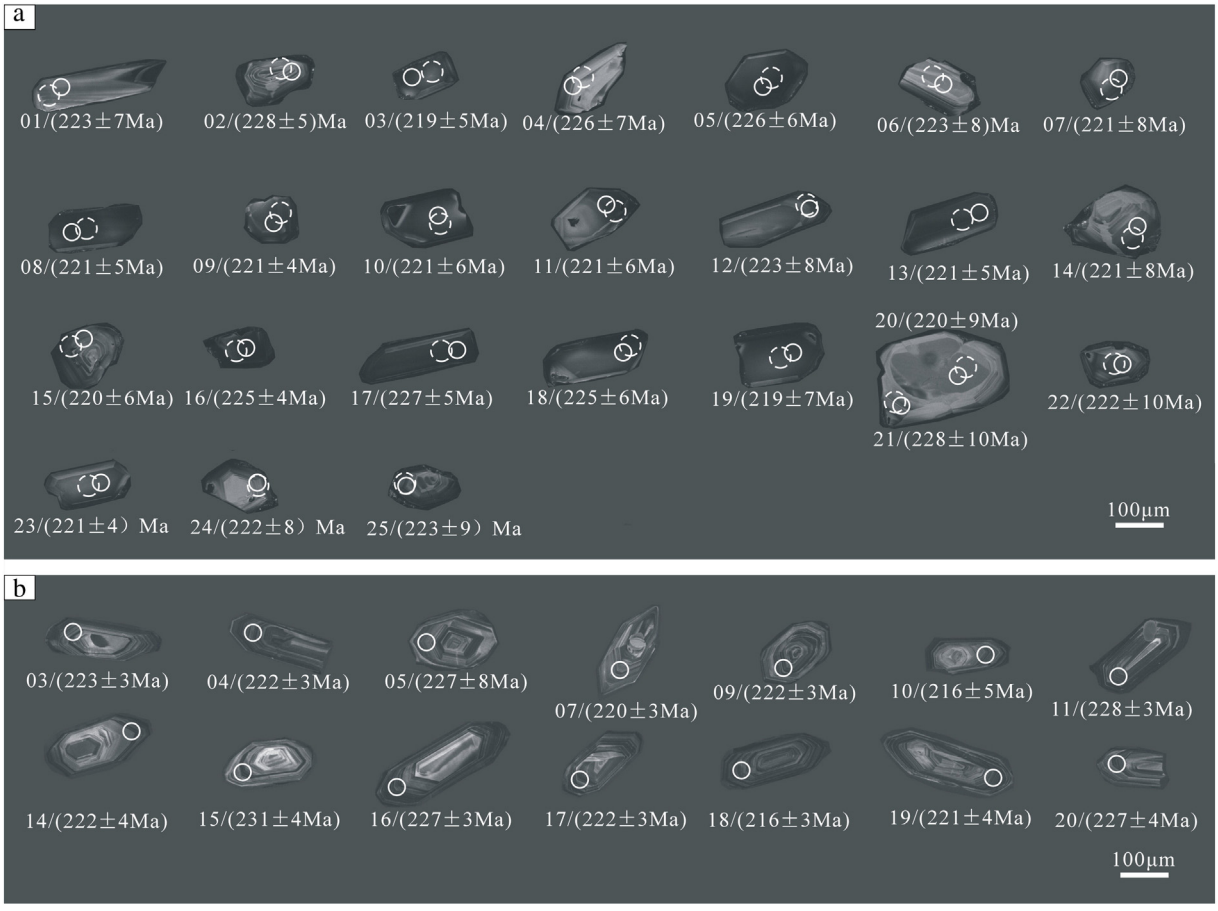

Fig. 6. Cathodoluminescence (CL) images of zircons from (a) medium- to fine-grained quartz diorite and (b) porphyritic quartz diorite of the Saishitang Cu deposit. Smaller circles denote the locations of U–Pb dating, whereas bigger dotted circles show the positions of Lu–Hf analyses.

Table 1
Laser ablation–inductively coupled plasma–mass spectrometry (LA–ICP–MS) zircon data for medium- to fine-grained quartz diorite and porphyritic quartz diorite of the Saishitang Cu deposit.

Analysis no.	Th	U	Th/U	Isotopic ratios				Age/Ma			
	ppm			$^{207}Pb/^{235}U$	1σ	$^{206}Pb/^{238}U$	1σ	$^{207}Pb/^{235}U$	1σ	$^{206}Pb/^{238}U$	1σ
ST05, medium- to fine-grained quartz diorite, 25 spots											
@1	106	117	0.91	0.2570	0.0274	0.0352	0.0011	232	22	223	7
@2	183	199	0.92	0.2511	0.0181	0.0360	0.0008	228	15	228	5
@3	140	148	0.95	0.2420	0.0205	0.0346	0.0008	220	17	219	5
@4	48	90	0.53	0.2219	0.0307	0.0358	0.0011	203	26	226	7
@5	148	161	0.92	0.2291	0.0220	0.0357	0.0010	209	18	226	6
@6	75	76	0.99	0.2506	0.0364	0.0352	0.0013	227	30	223	8
@7	66	109	0.61	0.2547	0.0316	0.0348	0.0013	230	26	221	8
@8	246	232	1.06	0.2432	0.0160	0.0349	0.0007	221	13	221	5
@9	361	320	1.13	0.2313	0.0137	0.0348	0.0007	211	11	221	4
@10	86	103	0.84	0.2441	0.0276	0.0349	0.0010	222	22	221	6
@11	80	114	0.70	0.2419	0.0236	0.0349	0.0009	220	19	221	6
@12	86	136	0.63	0.2469	0.0291	0.0352	0.0013	224	24	223	8
@13	405	306	1.32	0.2414	0.0167	0.0348	0.0008	220	14	221	5
@14	46	71	0.65	0.2362	0.0401	0.0348	0.0013	215	33	221	8
@15	91	135	0.67	0.2275	0.0227	0.0347	0.0009	208	19	220	6
@16	295	279	1.06	0.2458	0.0154	0.0356	0.0007	223	13	225	4
@17	160	175	0.92	0.2329	0.0189	0.0358	0.0008	213	16	227	5
@18	138	165	0.84	0.2421	0.0236	0.0355	0.0010	220	19	225	6
@19	103	115	0.90	0.2296	0.0298	0.0345	0.0012	210	25	219	7
@20	48	68	0.71	0.2443	0.0419	0.0350	0.0015	222	34	222	9
@21	47	89	0.53	0.2422	0.0459	0.0361	0.0017	220	37	228	10
@22	77	112	0.68	0.2450	0.0403	0.0350	0.0016	223	33	222	10
@23	255	220	1.16	0.2412	0.0159	0.0348	0.0007	219	13	221	4
@24	109	118	0.92	0.2602	0.0307	0.0350	0.0013	235	25	222	8
@25	107	152	0.70	0.2653	0.0355	0.0352	0.0015	239	28	223	9
ZK2523B-02, porphyritic quartz diorite, 14 spots											
@03	240	708	0.34	0.2587	0.0086	0.0351	0.0004	234	7	223	3
@04	225	836	0.27	0.2488	0.0070	0.0350	0.0005	226	6	222	3
@05	138	622	0.22	0.2435	0.0165	0.0359	0.0014	221	13	227	8
@07	158	447	0.35	0.2447	0.0090	0.0347	0.0005	222	7	220	3
@09	362	784	0.46	0.2489	0.0069	0.0351	0.0004	226	6	222	3
@10	166	659	0.25	0.2178	0.0152	0.0340	0.0008	200	13	216	5
@11	278	728	0.38	0.2662	0.0093	0.0361	0.0005	240	7	228	3
@14	113	353	0.32	0.2338	0.0107	0.0351	0.0006	213	9	222	4
@15	112	515	0.22	0.2650	0.0115	0.0364	0.0006	239	9	231	4
@16	613	1819	0.34	0.2618	0.0069	0.0359	0.0005	236	6	227	3
@17	286	855	0.33	0.2461	0.0080	0.0350	0.0005	223	6	222	3
@18	252	692	0.36	0.2479	0.0085	0.0340	0.0005	225	7	216	3
@19	141	393	0.36	0.2347	0.0106	0.0348	0.0006	214	9	221	4
@20	157	525	0.30	0.2633	0.0119	0.0358	0.0007	237	10	227	4

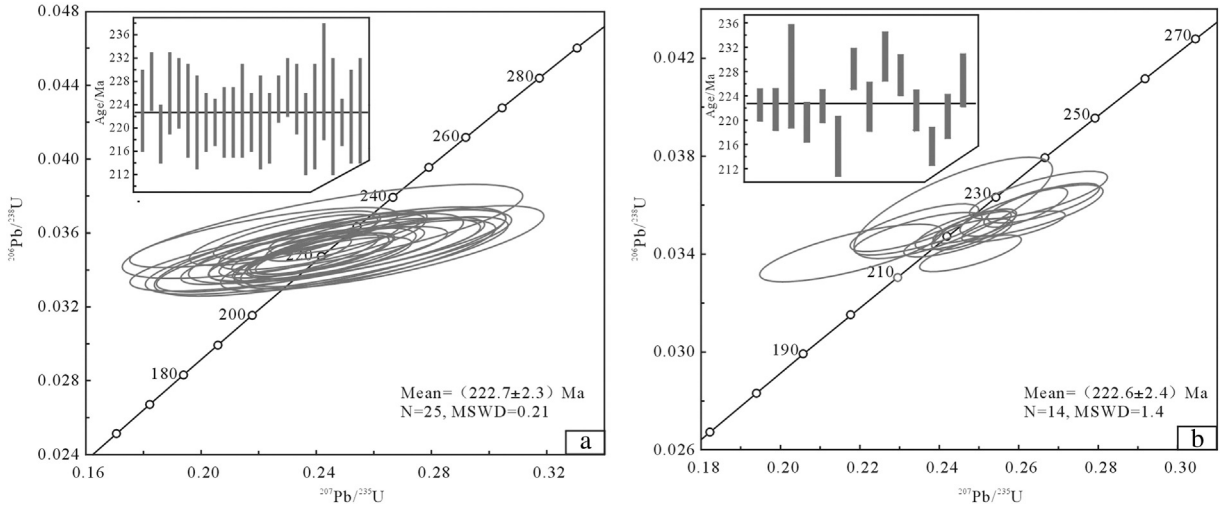

Fig. 7. Concordia diagrams of zircon U–Pb ages for (a) medium- to fine-grained quartz diorite and (b) porphyritic quartz diorite of the Saishitang Cu deposit.

Table 2
Re–Os isotopic data for molybdenite of the Saishitang Cu deposit.

Sample no.	Weight (mg)	Re ± 2σ (μg/g)	Os ± 2σ (ng/g)	^{187}Re ± 2σ (μg/g)	^{187}Os ± 2σ (ng/g)	Model age (Ma)
ZK019-1-1	10.04	4.495 ± 0.053	0.0161 ± 0.1085	2.825 ± 0.034	10.540 ± 0.120	223.5 ± 4.1
ZK019-2-1	50.55	4.184 ± 0.039	0.0025 ± 0.0093	2.630 ± 0.025	9.867 ± 0.083	224.8 ± 3.4
ZK019-2-2	22.92	1.942 ± 0.019	0.0017 ± 0.0019	1.221 ± 0.012	4.551 ± 0.035	223.4 ± 3.3
ZK019-3-1	5.11	8.588 ± 0.080	0.0029 ± 0.0033	5.397 ± 0.050	20.170 ± 0.160	223.9 ± 3.3
ZK019-3-2	6.34	0.583 ± 0.006	0.0035 ± 0.0039	0.366 ± 0.004	1.351 ± 0.013	221.0 ± 3.5

5. Analytical results

5.1. Zircon U–Pb ages

The results of zircon U–Pb dating of the medium- to fine-grained quartz diorite (ST05) and porphyritic quartz diorite (ZK2523B-02) are summarized in Fig. 6 and Table 1. Most of the analyzed zircon grains are euhedral and colorless, and exhibit weak or clear oscillatory growth zoning (Fig. 6). The Th/U ratios of ST05 and ZK2523B-02 are 0.53–1.32 and 0.22–0.46, respectively, indicating that the zircons are of magmatic origin (Hoskin and Schaltegger, 2003). For sample ST05, the ^{206}Pb/^{238}U ages from 25 spots range from 219 ± 7 Ma to 228 ± 7 Ma, with a weighted mean age of 222.7 ± 2.3 Ma (1σ, MSWD = 0.21, N = 25) (Fig. 7a). For sample ZK2523B-02, 14 of the 20 spots have concordant ^{206}Pb/^{238}U ages, which range from 216 ± 5 Ma to 228 ± 3 Ma, with a weighted mean age of 222.6 ± 2.4 Ma (1σ, MSWD = 1.4, N = 14) (Fig. 7b). These ages represent the timing of magma emplacement in the Saishitang Cu deposit.

5.2. Molybdenite Re–Os ages

The molybdenite Re–Os isotopic data of the Saishitang Cu deposit are listed in Table 2. Five samples show consistent model ages, ranging from 221.0 ± 1.5 to 224.8 ± 3.4 Ma, with a well-constrained ^{187}Re–^{187}Os isochron age of 224.5 ± 1.8 Ma (2σ, MSWD = 0.15; Fig. 8a) and a weighted average age of 223.4 ± 1.5 Ma (2σ, MSWD = 0.65) (Fig. 8b). Therefore, the isochron age (224.5 ± 1.8 Ma) represents the timing of mineralization.

5.3. Geochemical compositions of granitoids

Major and trace elemental compositions of the medium- to fine-grained quartz diorite (ST05, ST06, ST07, ST09-1, ST09-2 and ST09-3) and porphyritic quartz diorite (2021B03-18 and 2021B03-19) are listed in Table 3. The medium- to fine-grained quartz diorite (the inner phase) has a SiO_2 content of 59.63–62.65 wt.%, a K_2O content 1.65–2.49 wt.%, and an Al_2O_3 content of 16.84–18.13 wt.%. In contrast, the porphyritic quartz diorite (the outer phase) has higher SiO_2 (67.34–68.21 wt.%) and K_2O (3.17–3.34 wt.%), but lower Al_2O_3 (15.57–15.62 wt.%). The aluminum saturation index (A/CNK), Rittmann index (σ), and Mg# of all samples are similar, ranging from 0.86 to 1.01, 1.48 to 1.82, and 46 to 52, respectively.

On a K_2O vs. SiO_2 diagram (Fig. 9a), all samples fall in the medium-K to high-K calc-alkaline series and categorized as metaluminous (Fig. 9b). They show high total REE contents ($\sum$REE = 121.00–165.09 ppm), significant light rare earth element (LREE) enrichment (LREE/HREE = 7.36–13.03; $(La/Yb)_N$ = 8.17–20.43), and weak negative Eu anomalies (δEu = 0.69–0.86; Fig. 9c). Trace element spider diagrams (Fig. 9d) show the relative enrichment of Rb, Th, K, and Pb, and depletion of Nb, Ta, P, and Ti. The depletion of P and Ti indicate the fractional crystallization of apatite, sphene, and Ti-rich minerals. Quartz diorite in the Saishitang deposit display nearly identical REE and trace element patterns with the typical Late Triassic granitoids in the EKOB (Fig. 9c, d). The granitoids in Xiangride area have lower Sr, P, and Ti values, which may indicate greater differentiation during magmatic evolution.

5.4. Zircon Hf isotopes

In situ Hf isotopic analyses of zircons from the medium- to fine-grained quartz diorite sample (ST05, with ^{206}Pb/^{238}U ages of ca. 222.7 Ma) are shown in Fig. 6. The zircon Hf isotopic data and calculation results are presented in Table 4. The ^{176}Hf/^{177}Hf ratios range from 0.282580 to 0.282757, with $\varepsilon_{Hf}(t)$ values between −2.05 and 4.87 (mean = 1.01 ± 0.77), and crustal model ages (T^C_{DM}) between 997 and 1387 Ma (mean = 1195 ± 49 Ma).

6. Discussion

6.1. Age of magmatism and mineralization

The timing of magmatic and hydrothermal events is important for the understanding of ore deposits, from both academic and

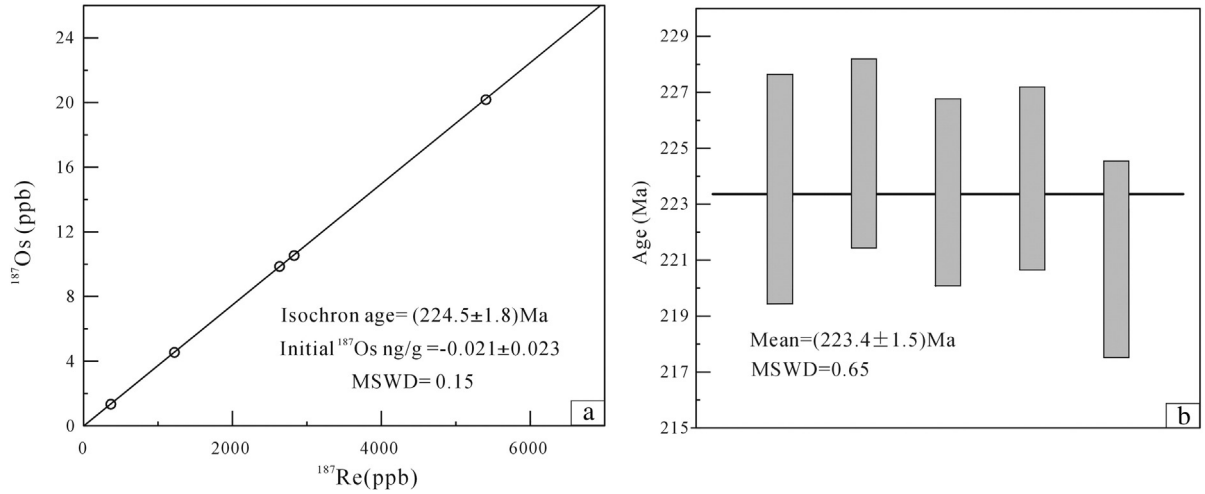

Fig. 8. (a) Re–Os isochron and (b) weighted mean model ages of molybdenite from the Saishitang Cu deposit.

Table 3
Geochemical compositions of quartz diorite from the Saishitang Cu deposit (major elements are presented in wt.%; trace elements are presented in ppm).

Sample no.	ST05	ST06	ST07	ST09-1	ST09-2	ST09-3	2021B03-18	2021B03-19
Rock type	Medium- to fine-grained quartz diorite						Porphyritic quartz diorite	
SiO_2 (%)	60.82	62.65	61.83	59.63	59.29	60.99	68.21	67.34
TiO_2 (%)	0.66	0.68	0.69	0.74	0.76	0.70	0.46	0.43
Al_2O_3 (%)	17.7	17.27	17.43	16.84	18.13	17.55	15.57	15.62
Fe_2O_3 (%)	1.19	0.97	0.91	0.94	0.88	0.50	0.37	0.20
FeO (%)	4.27	3.92	4.22	4.59	4.56	4.76	2.55	2.82
MnO (%)	0.09	0.09	0.09	0.09	0.08	0.09	0.04	0.05
MgO (%)	2.79	2.60	2.78	3.20	3.31	2.86	1.41	1.44
CaO (%)	5.40	5.02	5.40	6.76	6.82	5.89	4.02	3.77
Na_2O (%)	3.44	3.51	3.52	3.30	3.56	3.47	3.07	3.18
K_2O (%)	1.93	2.49	2.28	1.73	1.65	2.00	3.34	3.17
P_2O_5 (%)	0.20	0.14	0.13	0.15	0.24	0.16	0.07	0.12
F (%)	0.05	0.059	0.056	0.05	0.06	0.06	0.08	0.068
LOI (%)	1.13	0.93	0.92	1.17	0.78	1.08	0.72	0.65
Total	99.67	100.33	100.26	99.19	100.12	100.11	99.91	98.86
σ	1.82	1.77	1.48	1.65	1.64	1.62	1.63	1.50
Mg#	48	49	50	51	52	49	47	46
A/CNK	1.01	0.98	0.96	0.86	0.90	0.94	0.97	1.01
A/NK	2.28	2.04	2.11	2.31	2.37	2.23	1.80	1.80
Li (μg/g)	18.4	16.6	16.0	24.9	21.3	24.2	33.5	32.8
Be (μg/g)	1.65	1.65	1.72	1.52	1.53	1.66	2.08	2.13
Sc (μg/g)	15.1	14.2	17.1	17.2	18.3	15.9	8.81	8.95
V (μg/g)	97.1	76.4	81.6	113	121	101	45.4	42.8
Cr (μg/g)	42.3	24.3	27.1	27.0	31.4	29.9	23.8	20.1
Co (μg/g)	12.7	11.5	13	15.5	16.1	13.1	6.53	6.88
Ni (μg/g)	9.72	8.05	8.84	14.4	16.4	14	7.88	6.52
Cu (μg/g)	28.1	14.6	13.1	62.3	17.7	28.0	33.1	138
Zn (μg/g)	83.4	85.8	94.3	88.9	85.6	84.3	40.6	53.2
Ga (μg/g)	23.1	21.2	22.3	22.1	22.5	22.6	21.6	20.9
Rb (μg/g)	75.9	54.3	88.7	63.4	51.7	68.5	116	114
Sr (μg/g)	507	384	437	519	515	498	398	390
Y (μg/g)	19.2	22.4	23.9	23.8	21.6	21.7	17.3	18.3
Zr (μg/g)	85.6	175	125	159	148	166	149	141
Nb (μg/g)	9.13	10.3	10.5	8.54	8.62	9.26	12	11.8
Cs (μg/g)	7.12	5.63	6.02	4.05	3.20	4.55	7.47	6.38
Ba (μg/g)	722	627	695	595	623	686	737	760
Hf (μg/g)	2.3	4.58	3.49	4.27	3.97	4.37	4.13	4.24
Ta (μg/g)	0.78	0.84	0.88	0.68	0.64	0.72	1.38	1.57
Pb (μg/g)	12.1	13.8	14.8	20.7	14.6	18.1	12.6	15.5
Th (μg/g)	6.74	6.95	8.04	6.23	5.04	6.28	17.1	16.3
U (μg/g)	1.03	1.4	1.53	1.34	1.17	1.38	7.54	4.69
La (μg/g)	25.4	24.9	27.7	24.6	24.1	25.1	43.3	25.1
Ce (μg/g)	58.2	58.6	65	60.2	57.5	59.1	76.6	56.5
Pr (μg/g)	5.39	5.63	6.25	5.92	5.66	5.74	6.76	5.23
Nd (μg/g)	17.9	18.7	20.9	19.8	19.5	19.6	20.9	16.7
Sm (μg/g)	4.34	4.71	5.14	5.09	4.83	5.00	4.76	4.37
Eu (μg/g)	1.16	1.09	1.13	1.24	1.21	1.21	1	0.94
Gd (μg/g)	3.7	4.26	4.66	4.72	4.24	4.45	3.8	3.77
Tb (μg/g)	0.59	0.69	0.76	0.76	0.69	0.73	0.61	0.6
Dy (μg/g)	3.25	3.93	4.22	4.24	3.87	4.08	3.11	3.2
Ho (μg/g)	0.64	0.77	0.82	0.85	0.77	0.78	0.59	0.61
Er (μg/g)	1.93	2.3	2.47	2.49	2.25	2.28	1.69	1.8
Tm (μg/g)	0.27	0.33	0.33	0.34	0.31	0.31	0.23	0.26
Yb (μg/g)	1.73	2.08	2.15	2.16	2.01	1.99	1.52	1.67
Lu (μg/g)	0.26	0.31	0.32	0.32	0.30	0.30	0.22	0.25
∑REE	124.76	128.30	141.85	132.73	127.24	130.67	165.09	121.00
LREE	112.39	113.63	126.12	116.85	112.80	115.75	153.32	108.84
HREE	12.37	14.67	15.73	15.88	14.44	14.92	11.77	12.16
LREE/HREE	9.09	7.75	8.02	7.36	7.81	7.76	13.03	8.95
$(La/Yb)_N$	10.53	8.59	9.24	8.17	8.60	9.05	20.43	10.78
δEu	0.86	0.73	0.69	0.76	0.80	0.77	0.70	0.69
δCe	1.16	1.17	1.16	1.18	1.17	1.16	0.99	1.15

LOI = loss on ignition, $Mg\# = 100 \times Mg^{2+} / (Mg^{2+} + TFe^{2+})$; A/CNK = mole $[Al_2O_3/(CaO + Na_2O + K_2O)]$; A/NK = mole $[Al_2O_3/(Na_2O + K_2O)]$; $\sigma = (Na_2O + K_2O) \times 2 / (SiO_2 - 43)$ (wt.%); $\delta Eu = 2 \times w(Eu)_N / [w(Gd)_N + w(Sm)_N]$; $\delta Ce = 2 \times w(Ce)_N / [w(La)_N + w(Pr)_N]$; $(La/Yb)_N = (La/0.237)/(Yb/0.17)$.

exploration viewpoints (Stein et al., 1997). Previous chronological studies of the Saishitang intrusions obtained biotite K–Ar ages of 218–248 Ma (Li et al., 2009a). Liu et al. (2012a) reported zircon U–Pb ages of quartz diorite porphyry and granite porphyry of 223.2 ± 2.2 Ma and 219.9 ± 2.6 Ma, respectively. However, there are no precise age constraints for the quartz diorite as the main intrusions of the Saishitang deposit. The new dating results of the medium- to fine-grained quartz diorite (222.7 ± 2.3 Ma) and the porphyritic quartz diorite (222.6 ± 2.4 Ma) and molybdenite (224.5 ± 1.8 Ma) presented in this study are consistent with the past studies. The zircon U–Pb and molybdenite Re–Os ages are concordant within error limits. These ages constrain the timing of emplacement and the associated Cu mineralization in the Saishitang Cu deposit to the Late Triassic (~222 Ma).

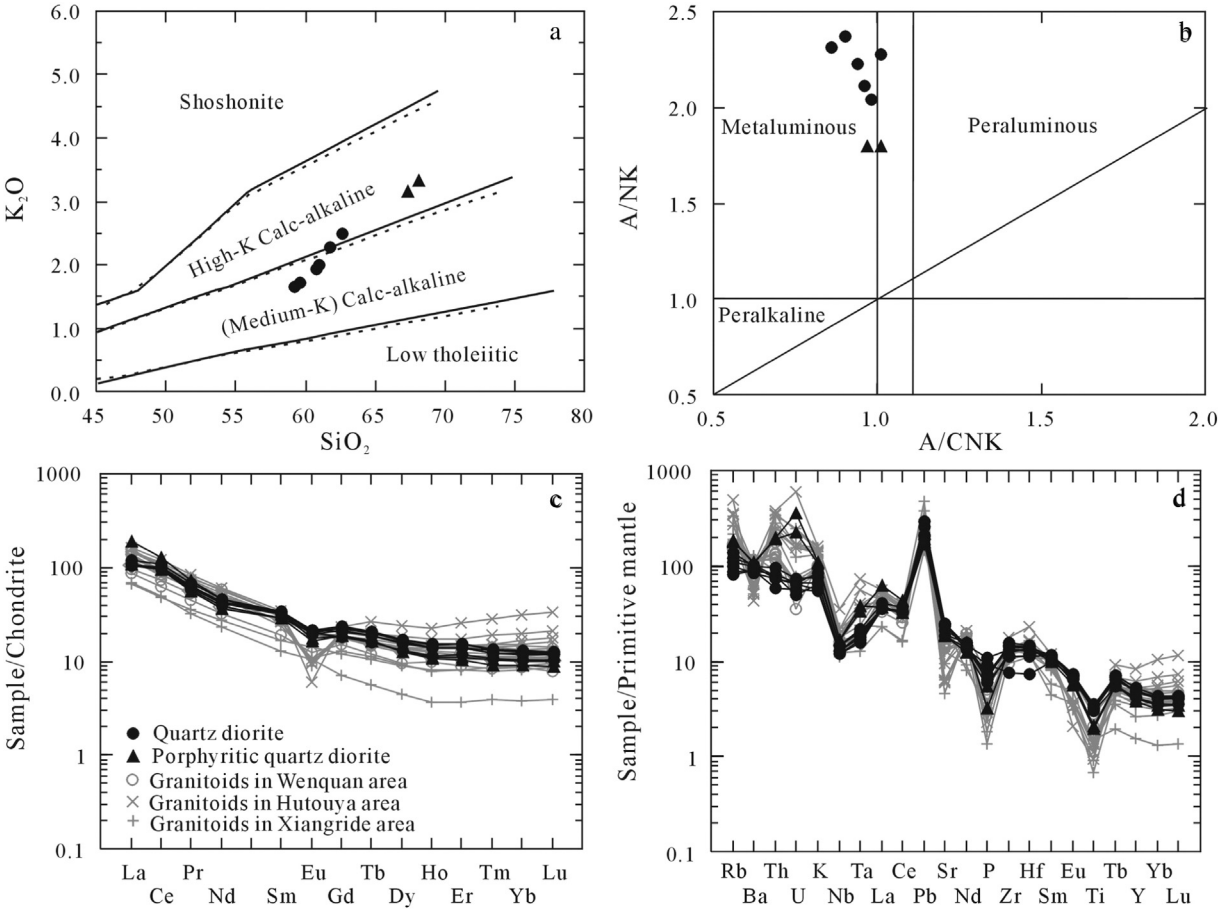

Fig. 9. Geochemical characterization of quartz diorite of the Saishitang Cu deposit. (a) SiO_2 vs. K_2O (Rickwood, 1989). (b) A/CNK vs. A/NK (Peccerillo and Taylor, 1976). (c) Chondrite-normalized rare earth element (REE) patterns. (d) Primitive-mantle-normalized spider diagram (chondrite and primitive-mantle values are from Sun and McDonough, 1989).

Four main orogenic cycles have been recognized in the EKOB (Mo et al., 2007): Precambrian, Early Paleozoic, Late Paleozoic–Early Mesozoic, and Late Mesozoic–Cenozoic. The third orogenic cycle is related to the most significant magmatic activity (260–200 Ma), accompanying large-scale mineralization. The results of this study show that the high-precision mineralization ages of Cu or Cu–polymetallic porphyry–skarn deposits in the EKOB all have mineralization ages of 240–220 Ma (Table 5). These results indicate that they formed in the late stage of the late Paleozoic–Early Mesozoic orogenic cycle.

6.2. Petrogenesis and sources of the granitoids

Identifying the genetic type of the granitoids is important for understanding the magma source, evolution, and tectonic setting (Pearce et al., 1984; Sylvester, 1998). In the Zr vs. 10,000 * Ga/Al and Ce vs. 10,000 * Ga/Al diagrams (Fig. 10a, b), quartz diorite samples of Saishitang deposit plot into the fields of I-, S-, or M-type granite. Furthermore, they are also high-SiO_2, medium-K to high-K calc-alkaline, metaluminous (A/CNK = 0.90–1.01), and have relatively high sodium contents (Na_2O = 3.07–3.56 wt.%, average value = 3.37 wt.%). These characteristics indicate that the quartz diorite of the Saishitang Cu deposit are I-type granite (Chappell and White, 1974), which is also supported by the presence of hornblende and the absence of cordierite and muscovite.

Experimental petrology has shown that high-K, calc-alkaline I-type granitoids are usually formed by the partial melting of hydrous calc-alkaline to high-K calc-alkaline, basaltic to intermediate metamorphic rocks within the crust (Patino-Douce and Harris, 1998; Patino-Douce and McCarty, 1998). There are no mafic rocks coexisting with the quartz diorite in the mining area and outside, precluding the possibility that quartz diorite was generated merely by the fractional crystallization of mafic magmas. Additionally, in the plot of Th/Nd vs. Th and Rb/Nd vs. Rb, the quartz diorite samples show a slope trend (Fig. 11a, b), suggesting partial melting or magma mixing is the dominant factor in the magma evolution.

Along with high SiO_2 (59.29–68.21 wt.%), Al_2O_3 (15.57–18.13 wt.%), and K_2O contents (1.65–3.34 wt.%) (Table 3), quartz diorite of the Saishitang Cu deposit display pronounced negative Nb, Ta, P, and Ti anomalies, but are enriched in Rb, Th, K, and Pb (Fig. 9d). These characteristics are consistent with typical crustal melts (Harris et al., 1986; Chappell and White, 1992; Bea et al., 2011). Previous studies show that elemental ratios, such as Nb/Ta ratios can be very useful in fingerprinting source regions (Eby et al., 1998). The Nb/Ta ratios of the quartz diorite range from 7.52 to 13.47, with an average value of 11.37, which is between the average value of upper crust (Nb/Ta = 13.4) and lower crust (Nb/Ta = 8.3; Rudnick and Gao, 2003), further favoring the crustal origin. The Mg# of a rock is a good indicator of whether the magma source is derived from crustal material alone or from crustal material contaminated by mantle material (Smithies and Champion, 2000). Melts that form by the partial melting of basaltic lower crust usually have a lower Mg# (<40) than those with an involvement from mantle material (Mg# > 40; Rapp and Watson, 1995). The high Mg# (46–52) values of the quartz diorite suggest that mantle components were involved in their genesis.

The Hf isotope data provide another important evidence for the source of the quartz diorite. The quartz diorite possess heterogeneous zircon Hf isotopic compositions, with $\varepsilon_{Hf}(t)$ values between −2.05 and 4.87 (up to 7 epsilon units) and in the $\varepsilon_{Hf}(t)$ vs. age figure (Fig. 12), the spots

Table 4
Hf isotopic data for zircons from medium- to fine-grained quartz diorite of the Saishitang deposit.

Analysis no.	$^{176}Yb/^{177}Hf$	$^{176}Lu/^{177}Hf$	$^{176}Hf/^{177}Hf$	1σ	$^{176}Hf/^{177}Hf_t$	$\varepsilon_{Hf}(0)$	$\varepsilon_{Hf}(t)$	T^C_{GM} (Ma)	$f_{Lu/Hf}$
ST05, medium- to fine-grained quartz diorite, 222.7 Ma									
@1	0.038660	0.000648	0.282649	0.000011	0.282646	−4.35	0.44	1228	−0.98
@2	0.084336	0.001365	0.282664	0.000012	0.282658	−3.82	0.87	1201	−0.96
@3	0.105176	0.001652	0.282747	0.000013	0.282740	−0.87	3.78	1016	−0.95
@4	0.047015	0.000768	0.282607	0.000012	0.282604	−5.85	−1.07	1325	−0.98
@5	0.086550	0.001431	0.282696	0.000013	0.282690	−2.70	1.99	1130	−0.96
@6	0.044141	0.000789	0.282647	0.000011	0.282644	−4.40	0.37	1233	−0.98
@7	0.044565	0.000741	0.282598	0.000012	0.282595	−6.15	−1.37	1344	−0.98
@8	0.047460	0.000785	0.282606	0.000022	0.282603	−5.87	−1.10	1326	−0.98
@9	0.130803	0.002032	0.282757	0.000013	0.282749	−0.53	4.07	997	−0.94
@10	0.081649	0.001287	0.282692	0.000012	0.282687	−2.83	1.87	1137	−0.96
@11	0.087029	0.001455	0.282638	0.000014	0.282632	−4.72	−0.05	1259	−0.96
@12	0.087137	0.001471	0.282661	0.000014	0.282655	−3.91	0.77	1208	−0.96
@13	0.130870	0.002009	0.282738	0.000014	0.282730	−1.21	3.39	1040	−0.94
@14	0.073424	0.001211	0.282667	0.000013	0.282662	−3.71	1.01	1192	−0.96
@15	0.062802	0.001067	0.282586	0.000013	0.282581	−6.59	−1.86	1375	−0.97
@16	0.135378	0.002127	0.282713	0.000013	0.282704	−2.09	2.49	1098	−0.94
@17	0.117098	0.001850	0.282739	0.000013	0.282731	−1.18	3.45	1037	−0.94
@18	0.075147	0.001254	0.282624	0.000014	0.282619	−5.24	−0.53	1290	−0.96
@19	0.127803	0.001994	0.282741	0.000014	0.282733	−1.10	3.50	1033	−0.94
@20	0.048438	0.000811	0.282644	0.000014	0.282640	−4.53	0.24	1241	−0.98
@21	0.065244	0.001098	0.282625	0.000014	0.282620	−5.21	−0.48	1287	−0.97
@22	0.062358	0.001036	0.282580	0.000012	0.282576	−6.79	−2.05	1387	−0.97
@23	0.134947	0.002122	0.282713	0.000014	0.282704	−2.09	2.49	1098	−0.94
@24	0.121348	0.001911	0.282718	0.000027	0.282710	−1.92	2.69	1085	−0.94
@25	0.109356	0.001728	0.282734	0.000028	0.282727	−1.33	3.30	1046	−0.95

$\varepsilon_{Hf}(0) = [(^{176}Hf/^{177}Hf)_S / (^{176}Hf/^{177}Hf)_{CHUR,0} - 1] \times 10^4$.
$\varepsilon_{Hf}(t) = [((^{176}Hf/^{177}Hf)_S - (^{176}Lu/^{177}Hf)_S \times (e^{\lambda t} - 1)) / ((^{176}Hf/^{177}Hf)_{CHUR,0} - (^{176}Lu/^{177}Hf)_{CHUR} \times (e^{\lambda t} - 1)) - 1] \times 10^4$.
$T_{DM} = 1 / \lambda \times \ln[1 + ((^{176}Hf/^{177}Hf)_S - (^{176}Hf/^{177}Hf)_{DM}) / ((^{176}Lu/^{177}Hf)_S - (^{176}Lu/^{177}Hf)_{DM})]$.
$T^C_{GM} = T_{DM} - (T_{DM} - t) \times ((fcc - fs) / (fcc - f_{DM}))$.
$f_{Lu/Hf} = (^{176}Lu/^{177}Hf)_S / (^{176}Lu/^{177}Hf)_{CHUR} - 1$.
Where, $(^{176}Lu/^{177}Hf)_S$ and $(^{176}Hf/^{177}Hf)_S$ are measured values of samples, $(^{176}Lu/^{177}Hf)_{CHUR} = 0.0332$ and $(^{176}Hf/^{177}Hf)_{CHUR,0} = 0.282772$ (Blichert-Toft and Albarède, 1997); t = crystallization time of zircon. $\lambda = 1.867 \times 10^{-11}$ year^{-1} (Soderlund et al., 2004) was used in the calculations.

fall close to the line of chondrite. The negative $\varepsilon_{Hf}(t)$ values represent the features of the crustal melt, and the positive Hf isotopic ratios are consistent with mantle components (Kemp et al., 2007; Li et al., 2009b). In addition, the quartz diorite has crustal model ages (T^C_{GM}) between 997 and 1387 Ma (mean = 1195 Ma), suggesting that crustal growth took place during the Mesoproterozoic in the EKOB. This age is consistent with the lower crust metamorphic basement beneath the EKOB. Therefore, the quartz diorite of Saishitang most likely originated from the partial melting of Mesoproterozoic lower crustal materials with involvement of mantle-derived magmas.

6.3. Ore genesis

Mineral systems are controlled by the evolution of the earth system, particularly by its progressive cooling and geodynamic evolution from plume-influenced tectonics to modern plate tectonics (Groves and Bierlein, 2007; Santosh and Pirajno, 2014). Obviously, an understanding of ore genesis may provide insights to better constrain the tectonic setting. As mentioned above, three main genetic models have been proposed for the Saishitang Cu deposit: skarn-type (QGT, 1983; Xin et al., 2013; Cheng et al., 2014; Wang et al., 2015), exhalative sedimentary-

Table 5
High-precision magmatic and mineralization ages for the porphyry–skarn copper–polymetallic deposits of East Kunlun.

Location	Deposit	Type (elements)	Analytical methods	Age (Ma)	Reference
The Qimantagh Mountains	Yazigou	Porphyry (Cu, Mo)	Molybdenite Re–Os	224.7 ± 3.4	Li et al. (2008)
			Zircon SHRIMP U–Pb	224.0 ± 1.6	
	Wulanwuzhuer	Porphyry (Cu, Mo)	Zircon SHRIMP U–Pb	215.1 ± 4.5	She et al. (2007)
	Kaerqueka	Skarn–porphyry (Cu, Pb, Zn)	Molybdenite Re–Os	238.8 ± 1.3	Feng et al. (2009)
			Zircon SHRIMP U–Pb	237 ± 2	Wang et al. (2009)
			Zircon SHRIMP U–Pb	227 ± 2	Feng et al. (2012)
	Hutouya	Skarn (Cu, Pb, Zn)	Molybdenite Re–Os	225.0 ± 4.0	Feng et al. (2011)
			Molybdenite Re–Os	230.1 ± 4.7	
			Zircon LA–ICP–MS U–Pb	235.4 ± 1.8	
			Zircon SHRIMP U–Pb	219.2 ± 1.4	
The Buerhanda Mountains	Harizha	Porphyry (Cu, Mo)	Zircon LA–ICP–MS U–Pb	234.5 ± 4.8	Song et al. (2013)
	Qingshuihedong	Porphyry (Cu, Mo)	Zircon LA–ICP–MS U–Pb	~224 Ma	Chen et al. (2013)
	Tuoketuo	Porphyry (Cu, Au)	Zircon LA–ICP–MS U–Pb	232.49 ± 0.93	Xia et al. (2014a)
				232.6 ± 1.2	
	Xiadeboli	Porphyry (Cu, Mo)	Zircon LA–ICP–MS U–Pb	244.2 ± 2.1	Liu et al. (2012b)
The Ela Mountains	Jiadanggen	Porphyry (Cu, Mo)	Zircon LA–ICP–MS U–Pb	227.2 ± 1.9	Li et al. (2014)
	Saishitang	Skarn (Cu)	Molybdenite Re–Os	224.5 ± 1.8	This paper
			Zircon LA–ICP–MS U–Pb	222.7 ± 2.3	
			Zircon LA–ICP–MS U–Pb	222.6 ± 2.4	
			Zircon LA–ICP–MS U–Pb	223.3 ± 2.2	Liu et al. (2012a)
			Zircon LA–ICP–MS U–Pb	219.9 ± 2.6	

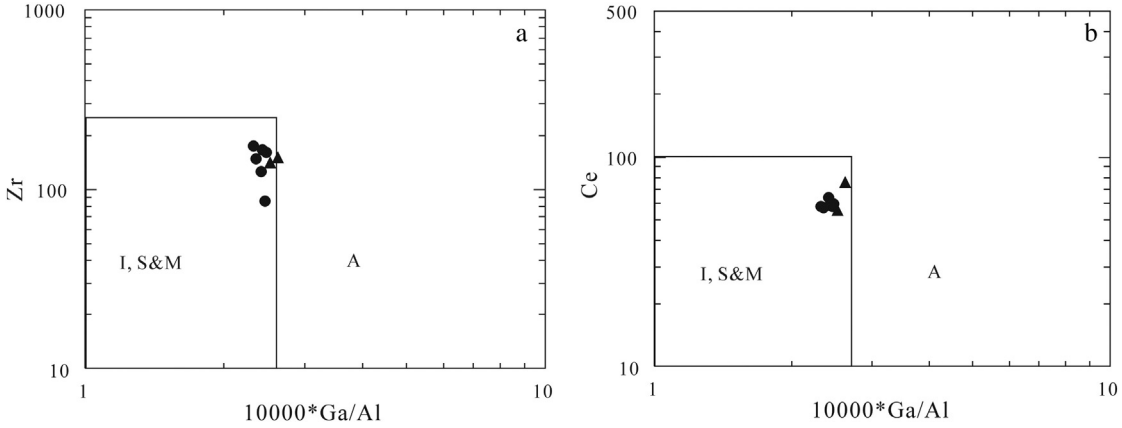

Fig. 10. (a) Zr vs. 10,000 * Ga/Al and (b) Ce vs. 10,000 * Ga/Al diagrams for quartz diorite of the Saishitang Cu deposit (Whalen et al., 1987). Symbols are as in Fig. 9.

type (Li et al., 1993; Song et al., 1995), and porphyry-type (Li et al., 2009a; Wu, 2010; Wei et al., 2012). Debate is focused on whether the stratiform skarns and orebodies were formed by exhalative sedimentary processes, and whether the disseminated mineralization in the intrusions is porphyry-type mineralization. The ore genesis is also crucial for determining key ore-controlling factors, and therefore for guiding exploration and prospecting. For porphyry- and skarn-type deposits, exploration should focus on the intrusions and on the contact zone between intrusions and wall-rock, whereas for exhalative sedimentary deposits, exploration should focus on the stratigraphic horizon. The results of this study suggest that the Saishitang Cu deposit is a skarn deposit. The evidence is discussed below.

(1) Field geological surveys and drill core logging reveal that the locations of orebodies were not strongly controlled by the wall-rock lithology. Some small-scale orebodies were also found in the metamorphosed tuff or in the marble near the main orebodies. The main orebodies of Saishitang Cu deposit are not stratiform, but are stratoid, lenticular, and veined (Liu et al., 2012a; Xin et al., 2013). Furthermore, most of the banded skarns, which was considered to originate from exhalative sedimentary processes, all contain the skarn veins that cut across sedimentary beds in which the skarn minerals crystallized almost contemporaneously (Fig. 5b). Therefore, the banded skarn appears to have resulted from the selective replacement of bedding in the wall rocks under the influence of hydrothermal fluids.

(2) The economic orebodies of the Saishitang deposit occur mainly in the contact zone between quartz diorite and Lower to Middle Triassic metamorphosed tuff and marble. Some non-economic orebodies (considered as porphyry-type) are also found within the intrusions. From the intrusions to the wall rocks, different alteration zones are recognized. These features indicate a clear link between the orebodies and intrusions, as demonstrated by the sulfur isotope data of sulfides ($\delta^{34}S$ values range from −4.82 to 4.11‰; Mao, 2012). The consistent zircon U–Pb and molybdenite Re–Os ages obtained in this study also suggest that ore formation was genetically related to the intrusions.

(3) The composition of skarn minerals reflects the physical and chemical environment in which they formed (Meinert et al., 2005), and it can therefore be used to constrain the genesis of the skarn. Most skarn deposits are characterized by two different alteration stages: an early stage that produced anhydrous minerals (e.g., garnet and pyroxene) and a retrograde skarn stage that produced hydrous minerals (e.g., amphibole and epidote; Kwak, 1994; Meinert et al., 2003). Typical intrusion-related prograde skarns consist mainly of andradite–grossularite garnet and diopside–hedenbergite pyroxene (Meinert et al., 2005).

Our previous study of the skarn minerals of the Saishitang deposit has recognized four stages of skarn and ore formation (Wang et al., 2015): (1) a prograde skarn stage, (2) a retrograde skarn stage, (3) a quartz–sulfide stage, and (4) a quartz–carbonate stage. The prograde skarn stage consists of garnet, pyroxene, and wollastonite, while the retrograde skarn stage is dominated by magnetite, amphibole, and epidote. Garnet and pyroxene have compositions of $Gro_{0.00–91.00}$ $And_{7.02–100.00}$ $(Pyr + Alm + Spe)_{0.00–4.27}$ and $Di_{12.80–91.75}$ $Hd_{2.41–79.80}$ $(Jo + Jd + Opx)_{0.00–13.47}$, respectively (Wang et al., 2015). The results suggest that the skarn of the Saishitang deposit is compositionally comparable to typical skarn deposits.

The quartz diorite of the Saishitang deposit is derived from partial melting of lower crust with the input of mantle-derived magmas. Previous study shows the mantle is one of important metal sources for

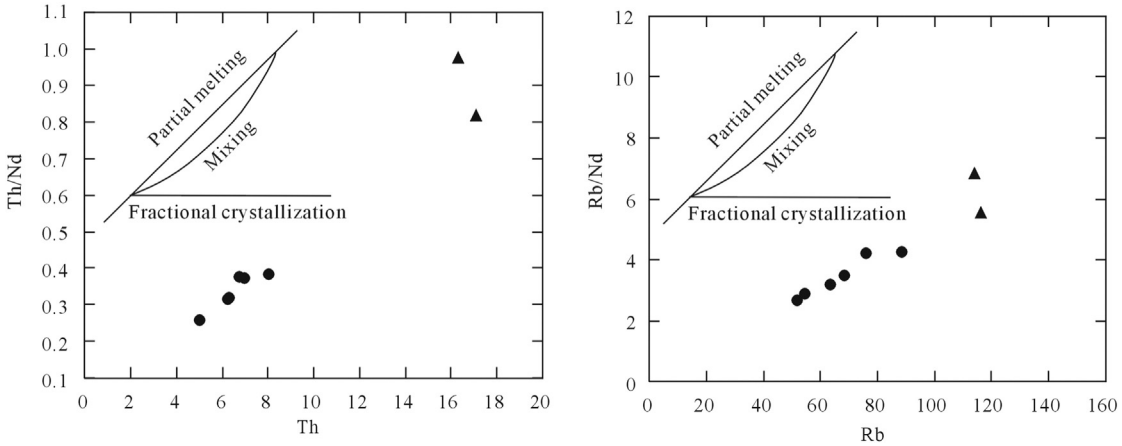

Fig. 11. (a) Th/Nd vs. Th and (b) Rb/Nd vs. Rb diagrams for quartz diorite of the Saishitang Cu deposit (Schiano et al., 2010). Symbols are as in Fig. 9.

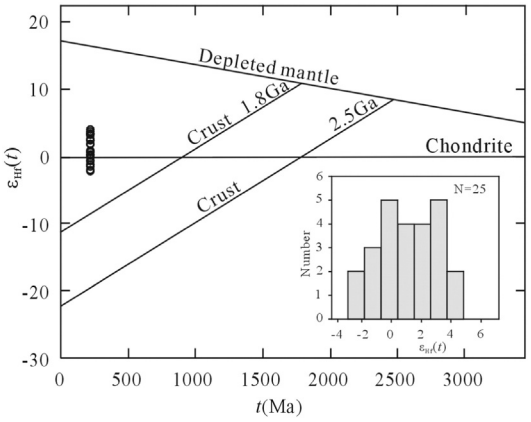

Fig. 12. Histograms of zircon $\varepsilon_{Hf}(t)$ values for zircons from medium- to fine-grained quartz diorite of the Saishitang Cu deposit.

Cu deposit (Mungall, 2002). For these reasons, we consider that the Saishitang Cu deposit is the product of a porphyry–skarn mineral system related to the extensive crust–mantle interaction.

6.4. Tectonic setting

The EKOB records a complex history of seafloor spreading, subduction, and continental collision extending back to the early Paleozoic (Jiang et al., 1992; Yang et al., 1996; Yin and Harrison, 2000), and records the widespread intrusion of granitoids during the late Permian–Triassic (Fig. 1c; Mo et al., 2007; Zhang et al., 2012). The Ela Mountain area is located in the easternmost part of the EKOB, near the WQOB in the east. The small branch (or aulacogen) of the Paleo-Tethys Ocean, between the EKOB and the WQOB, disappeared with the closure of the A'nyemaqen Ocean (Sun et al., 2004; Zhang et al., 2004b; Zhang, 2008). The granitoids in the Ela Mountain area show the same tectonic evolution history with the EKOB (Pan et al., 1997; Kui et al., 2010). As mentioned above, the magma emplacement and associated Cu mineralization happened in Late Triassic (~222 Ma). Combining this result with the regional tectonic setting, we infer that the Saishitang Cu deposit was formed in a post-collision setting, which is supported by the following lines of evidence.

(1) The distribution of the granitoids in the EKOB shows that the Late Permian to Middle Triassic granitoids have a linear distribution along the North Kunlun Fault (Luo et al., 2014), whereas the Late Triassic granitoids (230–210 Ma), including the Saishitang intrusions, have an obvious planar distribution and occur in all tectonic sectors extending to the WQOB (Huang et al., 2014; Luo et al., 2014; Wang et al., 2014). The model of slab break-off–underplating–mixing–delamination in the post-collision setting (Chen et al., 2005) may provide a reasonable interpretation for the Late Triassic magmatism in the EKOB.

Several typical Late Triassic granitoids in the EKOB which show similar features (as shown in Fig. 9c, d) to the Saishitang intrusions are also interpreted to have formed in the post-collision setting, including granitoids in Hutouya area (Feng et al., 2012), Xiangride area (Luo et al., 2014), and Wenquan area (Zhang et al., 2006). The quartz diorite of the Saishitang deposit is calc-alkaline I-type granite. Geochemical data suggest it is derived from partial melting of lower crust with the input of mantle-derived magmas. In Nb vs. Y and Rb vs. Y + Nb diagrams (Fig. 13), the quartz diorite, together with coeval EKOB granitoids, plot near the domains of VAG + Syn-COLG, and POG, suggesting they are probably generated in the same tectonic setting.

(2) The presence of Late Permian to Middle Triassic marine carbonate and clastic rocks in the EKOB (Cai et al., 2008; Zhang et al., 2012) suggests that the A'nyemaqen Ocean did not close until the late Permian or Middle Triassic. As mentioned above, there is an important angular unconformity between Late Triassic terrestrial volcanic rocks (Elashan Formation and Babaoshan Formation) and underlying marine sequence in the EKOB. The underlying marine sequence is characterized by strong deformation, whereas the overlying units above this angular unconformity show relatively weak deformation (Liu, 2011a). Similarly, in the Saishitang mining area, we have observed the strong fold and deformation in the Lower to Middle Triassic sediments but there are no obvious deformations in the Late Triassic intrusions.

The Elashan Formation is distributed discontinuously along the entire EKOB with lithologies including basalt, trachyandesite, trachyte, andesite, rhyolite and pyroclastic rocks. Recently, Hu et al. (2015) reported the coeval mafic dikes and rhyolitic volcanic rocks (collected from Elashan Formation) which emplaced in the Late Triassic (from 228 to 218 Ma) and the mafic dikes intruded the A-type granite batholith with the zircon U–Pb age of 227 Ma. They are considered as different products of the same thermal event associated with post-collisional extension and related orogenic collapse.

(3) The evolution of Triassic sedimentary basin in the EKOB provides another evidence for the tectonic setting. The study of provenance, geochemistry of sandstone and detrital zircon ages shows that Lower to Middle Triassic Hongshuichuan Formation was formed in a fore-arc basin of which the geochemical characteristics similar to active continental margin, whereas Late Triassic Babaoshan Formation represents the foreland basin environment (Yan et al., 2008; Li et al., 2012a; Yue,

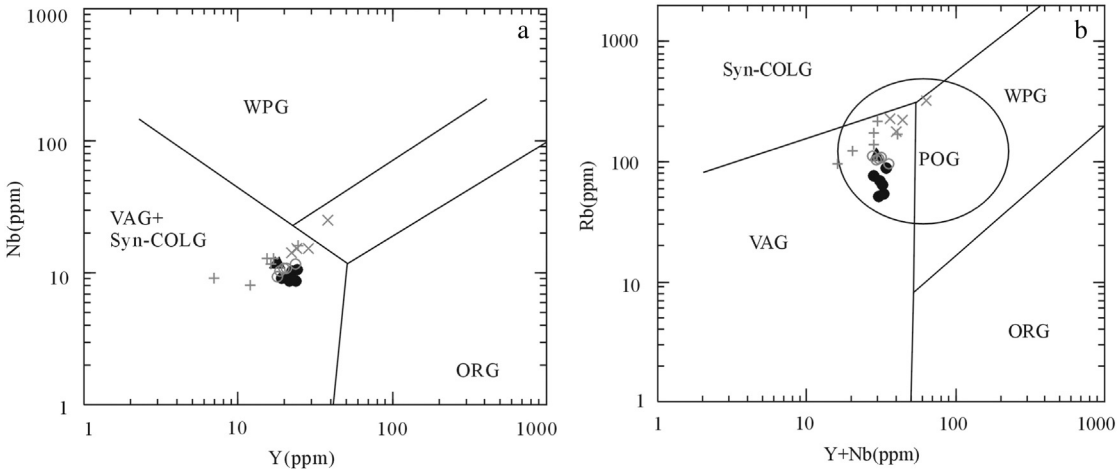

Fig. 13. Tectonic discrimination diagrams for quartz diorite of the Saishitang Cu deposit (Pearce et al., 1984). (a) Nb vs. Y. (b) Rb vs. (Y + Nb). Abbreviations: WPG = within-plate granites; VAG = volcanic arc granites; Syn-COLG = syn-collision granites; Post-COLG = post-collision granites; ORG = ocean ridge granites. Symbols are as in Fig. 9.

2014). The results suggest the A'nyemaqen Ocean was closed in the Middle–Late Triassic.

(4) A number of Late Triassic basaltic lavas with OIB geochemical affinities were identified in the EKOB, including the Binggou mafic dike swarms (226 Ma, Ma et al., 2013) in area, Xiahe basalt (220 Ma, Yan et al., 2012), and Manzhanggang mafic dike swarms (198 Ma, Sun et al., 2004). These gabbroic lavas probably indicate a regional extension setting related to post-collision.

The magmatic and sedimentary evidence discussed above suggest that the Saishitang Cu deposit was most likely formed in a post-collision setting. As demonstrated above, the quartz diorite of the Saishitang deposit is derived from partial melting of lower crust with the input of mantle-derived magmas. Underplating of mantle-derived magmas at the crust–mantle boundary is important in triggering crust–mantle interaction and mixing (e.g., Bergantz, 1989; Peressini et al., 2007). Thus, a likely scenario of the petrological and mineralization processes, as shown in Fig. 14, can be summarized as follows. The continued northward push from the Bayan Har terrane caused intense contraction and thickening of the lower crust beneath the EKOB (Guo et al., 1998; Zhang et al., 2011; Xia et al., 2014b). In a post-collision setting, the tectonic regime of regional extension in the EKOB induced the asthenosphere upwelling, which resulted in the hot mantle-derived melt underplating in the lower crust leading to crustal partial melting. Subsequently, the hybrid melts generated by the mantle-derived and lower crustal magmas, ascended to a shallow depth in the crust. The extensive crust–mantle interaction might have provided Cu and other metals into the magmatic system. With the emplacement of the intermediate-felsic magma, hydrothermal fluid exsolved from the magma caused extensive alteration, forming skarn and associated mineralization in the contact zone between quartz diorite and Lower to Middle Triassic rocks and minor porphyry-type mineralization within the intrusions.

Like the Saishitang Cu deposit, the porphyry–skarn Cu–polymetallic deposits of the EKOB (Table 5) all have similar mineralization ages (240–220 Ma). We infer that these deposits were formed mainly in post-collision setting, and are distinct from the porphyry–skarn Cu deposits generated in island- or continental-arc settings (Richards, 2003; Cooke et al., 2005). The results of this study indicate that the Late Triassic granitoids of the EKOB and adjacent areas have considerable potential for prospecting of porphyry–skarn Cu deposits.

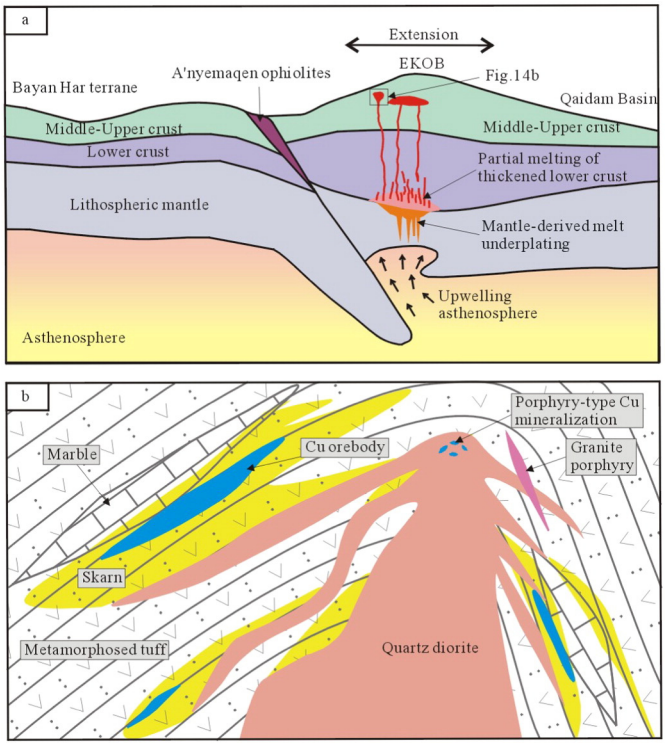

Fig. 14. Schematic cartoon illustrating a proposed genetic model and tectonic setting of the Saishitang Cu deposit.

7. Conclusions

(1) Molybdenite from the Saishitang Cu deposit yields an Re–Os age of 224.5 ± 1.8 Ma, while zircons from the medium- to fine-grained quartz diorite and porphyritic quartz diorite yield U–Pb ages of 222.7 ± 2.3 Ma and 222.6 ± 2.4 Ma, respectively, suggesting a close temporal relationship between magmatism and mineralization. Most of the porphyry–skarn Cu deposits in the EKOB have mineralization ages of 240–220 Ma.

(2) The geochemical data for the quartz diorite of the Saishitang Cu deposit indicate that it is calc-alkaline I-type granite which was probably derived from the partial melting of a thickened lower crust, with input of mantle components.

(3) The Saishitang Cu deposit is a skarn deposit with minor porphyry-type mineralization and the porphyry–skarn mineral system is related to the crust–mantle interaction.

(4) Based on the regional geology, the tectonic evolution, and geochemical evidence, the Saishitang Cu deposit is considered to be related to the regional extension of the EKOB during the Late Triassic, in a post-collision environment.

Acknowledgments

This study was supported by the Program of High-level Geological Talents (Grant No. 201309) and Youth Geological Talents (Grant No. 201112) of the China Geological Survey, and project No. 12120113093600 from the China Geological Survey. We thank Prof. Yueheng Yang for assistance with the zircon U–Pb analyses. Fieldwork was supported by Qinghai Saishitang Copper Corporation Ltd. We thank Prof. Franco Pirajno, Prof. Zhiming Yang and other anonymous reviewers for their valuable comments and suggestions to improve the paper.

References

Anderson, T., 2002. Correction of common lead in U–Pb analyses that do not report ^{204}Pb. Chem. Geol. 192, 59–79.
Bea, F., Mazhari, A., Montero, P., Amini, S., Ghalamghash, J., 2011. Zircon dating, Sr and Nd isotopes, and element geochemistry of the Khalifan pluton, NW Iran: evidence for Variscan magmatism in a supposedly Cimmerian superterrane. J. Asian Earth Sci. 40, 172–179.
Bergantz, G.W., 1989. Underplating and partial melting: implications for melt generation and extraction. Science 245, 1093–1095.
Blichert-Toft, J., Albarède, F., 1997. The Lu/Hf isotope geochemistry of chondrites and the evolution of the mantle–crust system. Earth Planet. Sci. Lett. 148, 243.
Cai, X.F., Luo, Z.J., Liu, D.M., Yuan, Y.M., 2008. The Xilikete Formation: an important lithostratigraphic unit of the Triassic system in the eastern Kunlun region. J. Stratigr. 32, 374–380 (in Chinese with English abstract).
Chappell, B.W., White, A.J.R., 1974. Two contrasting granite types. Pac. Geol. 8, 173–174.
Chappell, B.W., White, A.J.R., 1992. I- and S-type granites in the Lachlan Fold Belt. Trans. R. Soc. Edinb. Earth Sci. 83, 1–26.
Chen, H.W., Luo, Z.H., Mo, X.X., Liu, C.D., Ke, S., 2005. Underplating mechanism of Triassic granite of magma mixing origin in the East Kunlun Orogenic Belt. Geol. China 32, 386–395 (in Chinese with English abstract).
Chen, X.H., Gehrels, G., Yin, A., Li, L., Jiang, R.B., 2012. Paleozoic and Mesozoic basement magmatisms of Eastern Qaidam Basin, Northern Qinghai–Tibet Plateau: LA–ICP–MS zircon U–Pb geochronology and its geological significance. Acta Geol. Sin. 86, 350–369.
Chen, X.Y., Zhang, Y.L., Song, Z.B., Shu, X.F., Li, Y.Z., 2013. Geological and geochemical characteristics of Qingshuihe Donggou porphyry Cu–Mo deposit in East Kunlun. Geol. J. China Univ. 19, 357–358 (suppl., in Chinese).
Cheng, X.Y., Zhu, X.Y., Ding, T.Z., He, P., Wang, Y.L., 2014. Ore-controlling factors study of the Saishitang copper–polymetallic deposit, Qinghai Province. Miner. Explor. 5 (2), 233–241 (in Chinese with English abstract).
Cooke, D.R., Hollings, P., Walsh, J.L., 2005. Giant porphyry deposits: characteristics, distribution, and tectonic controls. Econ. Geol. 100 (5), 801–818.

Du, A.D., Wu, S.Q., Sun, D.Z., Wang, S.X., Qu, W.J., Markey, R., Stein, H., Morgan, J., Malinovskiy, D., 2004. Preparation and certification of Re–Os dating reference materials: molybdenite HLP and JDC. Geostand. Geoanal. Res. 28 (1), 41–52.
Eby, G.N., Woolley, A.R., Din, V., Platt, G., 1998. Geochemistry and petrogenesis of nepheline syenite: Kasungu–Chipala, Ilomba, and Ulindi nepheline syenite intrusions, North Nyasa Alkaline Province, Malawi. J. Petrol. 39, 1405–1424.
Feng, C.Y., Li, D.S., Qu, W.J., Du, A.D., Wang, S., Su, S.S., Jiang, J.H., 2009. Re–Os isotopic dating of molybdenite from the Suolajier skarn-type copper–molybdenum deposit of Qimantagh Mountain in Qinghai Province and its geological significance. Rock Miner. Anal. 28 (3), 223–227 (in Chinese with English abstract).
Feng, C.Y., Wang, S.P., Shu, X.F., Zhang, A.K., Xiao, Y., Liu, J.N., Ma, S.C., Li, G.C., Li, D.X., 2011. Isotopic chronology of the Hutouya skarn lead–zinc polymetallic ore district in Qimantagh area of Qinghai Province and its geological significance. J. Jilin Univ. (Earth Sci. Ed.) 41, 1806–1817 (in Chinese with English abstract).
Feng, C.Y., Wang, S., Li, G.C., Ma, S.C., Li, D.S., 2012. Middle to Late Triassic granitoids in the Qimantagh area, Qinghai Province, China: chronology, geochemistry and metallogenic significances. Acta Petrol. Sin. 28, 665–678 (in Chinese with English abstract).
Griffin, W.L., Pearson, N.J., Belousova, E., Jackson, S.E., Achterbergh, E., O'Reilly, S.Y., Shee, S.R., 2000. The Hf isotope composition of cratonic mantle: LA–MC–ICPMS analysis of zircon megacrysts in kimberlites. Geochim. Cosmochim. Acta 64, 133–147.
Griffin, W.L., Wang, X., Jackson, S.E., Pearson, N.J., O'Reilly, S.Y., Xu, X., Zhou, X., 2002. Zircon chemistry and magma mixing, SE China: in-situ analysis of Hf isotopes, Tonglu and Pingtan igneous complexes. Lithos 61, 237–269.
Griffin, W.L., Powell, W.J., Pearson, N.J., O'Reilly, S.Y., 2008. GLITTER: data reduction software for laser ablation ICP–MS. In: Sylvester, P. (Ed.), Laser Ablation–ICP–MS in the Earth Sciences: Current Practices and Outstanding Issues. Mineral. Assoc. Canada Short Course 40, pp. 308–311.
Groves, D.I., Bierlein, F.P., 2007. Geodynamic settings of mineral deposit systems. J. Geol. Soc. 164, 19–30.
Gu, X.P., Xie, X.D., Wu, X.B., Zhu, G.C., Lai, J.Q., Hoshino, K., Huang, J.W., 2012. Ferrisepiolite: a new mineral from Saishitang copper skarn deposit in Xinghai County, Qinghai Province, China. Eur. J. Mineral. 25, 177–186.
Guo, Z.F., Deng, J.F., Xu, Z.Q., Mo, X.X., Luo, Z.H., 1998. Late Palaeozoic–Mesozoic intracontinental orogenic process and intermediate-acidic igneous rocks from the eastern Kunlun. J. Grad. Sch. China Univ. Geosci. 12 (3), 234–352 (in Chinese with English abstract).
Harris, N.B.W., Pearce, J.A., Tindle, A.G., 1986. Geochemical characteristics of collision zone magmatism. In: Coward, M.P., Ries, A.C. (Eds.), Collision Tectonics. Spec. Publ., Geol. Soc. London, pp. 67–81.
Hoskin, P.W.O., Schaltegger, U., 2003. The composition of zircon and igneous and metamorphic petrogenesis. Rev. Mineral. Geochem. 53, 27–62.
Hou, Z.Q., Zheng, Y., Yang, Z., Rui, Z., Zhao, Z., Jiang, S., Qu, X., Sun, Q., 2013. Contribution of mantle components within juvenile lower-crust to collisional zone porphyry Cu systems in Tibet. Mineral. Deposita 48, 173–192.
Hu, Y., Niu, Y.L., Li, J.Y., Ye, L., Kong, J.J., Chen, S., Zhang, Y., Zhang, G.R., 2015. Petrogenesis and tectonic significance of the Late Triassic mafic dikes and felsic volcanic rocks in the East Kunlun Orogenic Belt, Northern Tibet Plate. Lithos http://dx.doi.org/10.1016/j.lithos.2015.05.004.
Huang, X.F., Mo, X.X., Yu, X.H., Li, X.W., Yang, M.C., Luo, M.F., He, W.Y., Yu, J.C., 2014. Origin and geodynamic settings of the Indosinian high Sr/Y granitoids in the West Qinling: an example from the Shehaliji pluton in Tongren area. Acta Petrol. Sin. 30 (11), 3255–3270 (in Chinese with English abstract).
Jiang, C.F., Yang, J.S., Feng, B.G., Zhu, Z.Z., Zhao, M., Chai, Y.C., 1992. Opening–Closing Tectonics of Kunlun Mountains. Geological Publishing House, Beijing, pp. 183–217 (in Chinese with English abstract).
Kemp, A.I.S., Hawkesworth, C.J., Foster, G.L., Paterson, B.A., Woodhead, J.D., Hergt, J.M., Gray, C.M., Whitehouse, M.J., 2007. Magmatic and crustal differentiation history of granitic rocks from Hf–O isotopes in zircon. Science 315, 980–983.
Kui, M.J., Bai, H.X., Gu, F.B., Miao, G.W., 2010. Division of East Kunlun tectonic magmatic belt and the rock tectonic combination in the late Variscan–Yanshanian period. J. Qinghai Univ. (Nat. Sci.) 28 (5), 49–55.
Kwak, T.A.P., 1994. Hydrothermal alteration in carbonate replacement deposits. Geological Association of Canada, Short Course Notes 11 pp. 381–402.
Lai, J.Q., An, J.H., Wang, X.J., Mao, Y., Song, Z.Y., Cao, Y.H., Tao, J.J., Guo, Z.J., Wang, J., 2010. Geochemical characteristics and tectonic environment analysis of the intrusive rocks in Saishitang ore field. Miner. Res. Geol. 24 (5), 460–465 (in Chinese with English abstract).
Li, F.D., Zhang, H.W., Song, Z.J., Su, Z.L., Liu, R.M., Li, W.M., 1993. The Ngola Shan Region Paleothermal Mineralization Pattern. Xi'an Jiaotong University Press, Xi'an, pp. 1–312 (in Chinese).
Li, S.J., Sun, F.Y., Feng, C.Y., Liu, Z.H., Zhao, J.W., Li, Y.C., Wang, S., 2008. Geochronological study on Yazigou polymetallic deposit in Eastern Kunlun, Qinghai Province. Acta Geol. Sin. 82 (7), 949–955 (in Chinese with English abstract).
Li, D.S., Kui, M.J., Gu, F.B., Wang, J.J., Bai, H.X., Zhan, F.Y., Wang, F.M., Ma, Y.Q., 2009a. Geological characteristics and genesis of the Saishitang copper deposit in Qinghai Province. Acta Geol. Sin. 83 (5), 719–730 (in Chinese with English abstract).
Li, X.H., Li, W.X., Wang, X.C., Li, Q.L., Liu, Y., Tang, G.Q., 2009b. Role of mantle-derived magma in genesis of early Yanshanian granites in the Nanling Range, South China: in situ zircon Hf–O isotopic constraints. Sci. China Ser. D Earth Sci. 39, 872–887.
Li, D.X., Feng, C.Y., Zhao, Y.M., Li, Z.F., Liu, J.N., Xiao, Y., 2011. Mineralization and alteration types and skarn mineralogy of Kaerqueka copper polymetallic deposit in Qinghai Province. J. Jilin Univ. (Earth Sci. Ed.) 41 (6), 1818–1830 (in Chinese with English abstract).
Li, R.B., Pei, X.Z., Li, Z.C., Liu, Z.Q., Chen, G.C., Chen, Y.X., Wei, F.H., Gao, J.M., Liu, C.J., Pei, L., 2012a. Geological characteristics of Late Paleozoic–Mesozoic unconformities and their response to some significant tectonic events in eastern part of Eastern Kunlun. Earth Sci. Front. 19, 244–254 (in Chinese with English Abstract).
Li, L.G., Liu, H., Yang, Z.X., Pan, Q., 2012b. Geological characteristics and deep prospecting evaluation in Saishitang copper deposit. Nonferrous Met. (Min. Sect.) 64 (2), 39–42 (in Chinese with English abstract).
Li, W., Neubauer, F., Liu, Y.J., Genser, J., Ren, S.M., Han, G.Q., Liang, C.Y., 2013. Paleozoic evolution of the Qimantagh magmatic arcs, Eastern Kunlun Mountains: constraints from zircon dating of granitoids and modern river sands. J. Asian Earth Sci. 77, 183–202.
Li, B.L., Zhi, Y.B., Zhang, L., Ding, Q.F., Xu, Q.L., Zhang, Y.J., Qian, Y., Wang, G., Peng, B., Ao, C., 2014. U–Pb dating, geochemistry, and Sr–Nd isotopic composition of a granodiorite porphyry from the Jiadanggen Cu–(Mo) deposit in the Eastern Kunlun Metallogenic Belt, Qinghai Province, China. Ore Geol. Rev. 67, 1–10.
Li, X.W., Huang, X.F., Luo, M.F., Dong, G.C., Mo, X.X., 2015. Petrogenesis and geodynamic implications of the Mid-Triassic lavas from East Kunlun, northern Tibetan Plateau. J. Asian Earth Sci. 105, 32–47.
Liu, Z., 2011. Structural features and their evolution of late Paleozoic to early Mesozoic stratigraphy in Alake Lake—Hongshuichuan area, East Kunlun region (Master Degree Thesis), Chang'an University, pp. 1–74 (in Chinese with English abstract).
Liu, C.D., Mo, X.X., Luo, Z.H., Yu, X.H., Chen, H.W., Li, S.W., Zhao, X., 2004. Mixing events between the crust- and mantle-derived magmas in Eastern Kunlun: evidence from zircon SHRIMP II chronology. Chin. Sci. Bull. 49, 828–834.
Liu, Z.Q., Pei, X.Z., Li, R.B., Li, Z.C., Zhang, X.F., Liu, Z.G., Chen, G.C., Chen, Y.X., Ding, S.P., Guo, J.F., 2011. LA–ICP–MS zircon U–Pb geochronology of the two suites of ophiolites at the Buqingshan area of the A'nyemaqen Orogenic Belt in the southern margin of East Kunlun and its tectonic implication. Acta Geol. Sin. 85, 185–194 (in Chinese with English abstract).
Liu, J.P., Lai, J.Q., Gu, X.P., Wang, X.J., Mao, Y., Song, W.B., 2012a. Geochemistry and zircon LA–ICPMS U–Pb geochronology of intrusive body in Saishitang copper deposit, Qinghai Province, China. Chin. J. Nonferrous Met. 22 (3), 622–632 (in Chinese with English abstract).
Liu, J.N., Feng, C.Y., Qi, F., Li, G.C., Ma, S.C., Xiao, Y., 2012b. SIMS zircon U–Pb dating and fluid inclusion studies of Xiadeboli Cu–Mo ore district in Dulan County, Qinghai Province, China. Acta Petrol. Sin. 28 (2), 679–690.
Lu, S.N., Li, H.K., Wang, H.C., Chen, Z.H., Zheng, J.K., Xiang, Z.Q., 2009. Detrital zircon population of Proterozoic meta-sedimentary strata in the Qinling–Qilian–Kunlun Orogen. Acta Petrol. Sin. 25, 2195–2208 (in Chinese with English abstract).
Ludwig, K.R., 2003. Isoplot 3.0, a geochronological toolkit for Microsoft Excel. Berkeley Geochronology Center. Spec. Publ. 4 pp. 1–71.
Luo, M.F., Mo, X.X., Yu, X.H., Li, X.W., Huang, X.F., Yu, J.C., 2014. Zircon LA–ICP–MS U–Pb age dating, petrogenesis and tectonic implications of the Late Triassic granites from the Xiangride area, East Kunlun. Acta Petrol. Sin. 30 (11), 3229–3241 (in Chinese with English abstract).
Ma, C.Q., Xiong, F.H., Zhang, J.Y., Liu, B., Huang, J., Jiang, H.A., 2013. Influence of the subducted slab from slab subduction to post-orogenic stage: the evidence from Early Permian–Late Triassic mafic dike swarms in the East Kunlun. Acta Geol. Sin. 87, 79–81 (suppl., in Chinese).
Mao, Y., 2012. Study on Stable Isotope, Fluid Inclusions and Mineralization of Saishitang Cu–Polymetallic Deposit, Qinghai Province (Master Degree Thesis), Central South University, Changsha, pp. 1–67 (in Chinese with English abstract).
Mao, J.W., Zhou, Z.H., Feng, C.Y., Wang, Y.T., Zhang, C.Q., Peng, H.J., Yu, M., 2012. A preliminary study of the Triassic large-scale mineralization in China and its geodynamic setting. Geol. China 39 (6), 1437–1471.
Mao, J.W., Luo, M.C., Xie, G.Q., Liu, J., Wu, S.H., 2014. Basic characteristics and new advances in research and exploration on porphyry copper deposits. Acta Petrol. Sin. 88 (12), 2153–2175 (in Chinese with English abstract).
Meinert, L.D., Hedenquist, J.W., Satoh, H., Matsuhisa, Y., 2003. Formation of anhydrous and hydrous skarn in Cu–Au ore deposits by magmatic fluids. Econ. Geol. 98, 147–156.
Meinert, L.D., Dipple, G.M., Nicolescu, S., 2005. World skarn deposits. Econ. Geol. 100th Anniversary, 299–336.
Mo, X.X., Luo, Z.H., Deng, J.F., Yu, X.H., Liu, C.D., Chen, H.W., Yuan, W.M., Liu, Y.H., 2007. Granitoids and crustal growth in the East-Kunlun Orogenic Belt. Geol. J. China Univ. 13 (3), 403–414 (in Chinese with English abstract).
Mungall, J.E., 2002. Roasting the mantle: slab melting and the genesis of major Au and Au-rich Cu deposits. Geology 30 (10), 915–918.
Nowell, G.M., Kempton, P.D., Noble, S.R., Fitton, J.G., Sauders, A.D., Mahoney, J.J., Taylor, R.N., 1998. High precision Hf isotope measurements of MORB and OIB by thermal ionization mass spectrometry: insights into the depleted mantle. Chem. Geol. 149, 211–233.
Pan, G.T., Chen, Z.L., Li, X.Z., Yan, Y.J., Xu, X.S., Xu, Q., Jiang, X.S., Wu, Y.L., Luo, J.N., Zhu, T.X., Peng, Y.M., 1997. Geological–Tectonic Evolution in the Eastern Tethys. Geological Publishing House, Beijing, pp. 1–218 (in Chinese).
Pan, G., Ding, J., Yao, D., Wang, L., compilers. 2004. Guidebook of 1:1,500,000 Geologic Map of the Qinghai–Xizang (Tibet) Plateau and Adjacent Areas. Chengdu Cartographic Publishing House, Chengdu, pp. 1–48 (in Chinese).
Patino-Douce, A.E., Harris, N., 1998. Experimental constraints on Himalayan anatexis. J. Petrol. 39, 689–710.
Patino-Douce, A.E., McCarty, T.C., 1998. Melting of crustal rocks during continental collision and subduction. In: Hacker, B.R., Liu, J.G. (Eds.), When Continents Collide: Geodynamics of Ultrahigh Pressure Rocks. Kluwer Academic Publisher, Netherlands, pp. 27–55.
Pearce, J.A., Harris, N.B.W., Tindle, A.G., 1984. Trace element discrimination diagrams for the tectonic interpretation of granitic rocks. J. Petrol. 25, 956–983.
Peccerillo, R., Taylor, S.R., 1976. Geochemistry of Eocene calc-alkaline volcanic rocks from the Kastamonu area, northern Turkey. Contrib. Mineral. Petrol. 58 (1), 63–81.
Peressini, G., Quick, J.E., Sinigoi, S., Hofmann, A.W., Fanning, M., 2007. Duration of a large mafic intrusion and heat transfer in the lower crust: a SHRIMP U–Pb zircon study in the Ivrea–Verbano Zone (Western Alps, Italy). J. Petrol. 48, 1185–1218.

Pirajno, F., Zhou, T.F., 2015. Intracontinental porphyry and porphyry–skarn mineral systems in eastern China: scrutiny of a special case "made-in-China". Econ. Geol. 110, 603–629.
Qinghai No. 3 Geological Team (QGT), 1983. Primary geological prospecting report of Saishitang copper deposit. Reports From Qinghai No. 3 Geological Team (QGT). pp. 1–134 (in Chinese).
Rapp, R.P., Watson, E.B., 1995. Dehydration melting of metabasalt at 8 ~ 32 kbar: implications for continental growth and crust–mantle recycling. J. Petrol. 36 (4), 891–931.
Richards, J.P., 2003. Tectono-magmatic precursors for porphyry Cu–(Mo–Au) deposit formation. Econ. Geol. 98, 1515–1533.
Richards, J.P., 2009. Postsubduction porphyry Cu–Au and epithermal Au deposits: products of remelting of subduction-modified lithosphere. Geology 37, 247–250.
Rickwood, P.C., 1989. Boundary lines within petrologic diagram which use oxides of major and minor elements. Lithos 22 (4), 247–263.
Rudnick, R.L., Gao, S., 2003. Composition of the continental crust. In: Heinrich, D.H., Karl, K.T. (Eds.), Treatise on Geochemistry. Pergamon, Oxford, pp. 1–64.
Santosh, M., Pirajno, F., 2014. Ore deposits in relation to solid Earth dynamics and surface environment: preface. Ore Geol. Rev. 56, 373–375.
Schiano, P., Monzier, M., Eissen, J.P., Martin, H., Koga, T., 2010. Simple mixing as the major control of the evolution of volcanic suites in the Ecuadorian Andes. Contrib. Mineral. Petrol. 160 (2), 297–312.
She, H.Q., Zhang, D.Q., Jiang, X.Y., Guan, J., Zhu, H.P., Feng, C.Y., Li, D.X., 2007. Geological characteristics and genesis of the Ulan Uzhur porphyry copper deposit in Qinghai. Geol. China 34 (2), 306–314 (in Chinese with English abstract).
Shirey, S.B., Walker, R.J., 1995. Carius tube digestion for low-blank rhenium–osmium analysis. Anal. Chem. 67, 2136–2141.
Smithies, R.H., Champion, D.C., 2000. The Archaean high-Mg diorite suite: links to tonalite–trondhjemite–granodiorite magmatism and implications for Early Archaean crustal growth. J. Petrol. 41 (12), 1653–1671.
Smoliar, M.I., Walker, R.J., Morgan, J.W., 1996. Re–Os ages of Group IIA, IIIA, IVA, and IVB iron meteorites. Science 271, 1099–1102.
Soderlund, U., Patchett, P.J., Vervoort, J.D., Isachsen, C.E., 2004. The ^{176}Lu decay constant determined by Lu–Hf and U–Pb isotope systematics of Precambrian mafic intrusions. Earth Planet. Sci. Lett. 219, 311–324.
Song, Z.J., Zhang, H.W., Li, W.M., Zhang, X.G., Wang, W., 1995. Metallogenic conditions and model of copper polymetallic deposit in Ngola San region, Qinghai Province. Northwest. Geosci. 16 (1), 134–144 (in Chinese with English abstract).
Song, Z.B., Zhang, Y.L., Chen, X.Y., Jiang, L., Li, D.S., Shu, X.F., Li, Y.Z., Li, J.C., Kong, H.L., 2013. Geochemical characteristics of Harizha granite diorite–porphyry in East Kunlun and their geological implications. Mineral Deposits 32 (1), 157–168 (in Chinese with English abstract).
Stein, H.J., Markey, R.J., Morgan, J.W., Du, A., Sun, Y., 1997. Highly precise and accurate Re–Os ages for molybdenite from the East Qinling molybdenum belt, Shanxi Province, China. Econ. Geol. 92, 827–835.
Sun, S.S., McDonough, W.F., 1989. Chemical and isotopic systematics of oceanic basalts: implications for mantle composition and processes. In: Saunders, A.D., Norry, M.J. (Eds.), Magmatism in the Ocean Basins. Geol. Soc. Spec. Publ., London 42, pp. 313–345.
Sun, Y.G., Zhang, G.W., Guo, A.L., Wang, J., 2004. Qinling–Kunlun triple junction and isotope chronological evidence of its tectonic processes. Geol. China 31 (4), 372–378 (in Chinese with English abstract).
Sylvester, P.J., 1998. Post-collisional strongly peraluminous granites. Lithos 45, 29–44.
Wang, G.C., Wei, Q.R., Jia, C.X., Zhang, K.X., Li, D.W., Zhu, Y.H., Xiang, S.Y., 2007. Some ideas of Precambrian geology in the East Kunlun, China. Geol. Bull. China 26, 929–937 (in Chinese with English abstract).
Wang, S., Feng, C.Y., Li, S.J., Jiang, J.H., Li, D.S., Su, S.S., 2009. Zircon SHRIMP U–Pb dating of granodiorite in the Kaerqueka polymetallic ore deposit, Qimantagh Mountain, Qinghai Province, and its geological implications. Geol. China 36 (1), 74–84 (in Chinese with English abstract).
Wang, B.Z., Chen, J., Luo, Z.H., Chen, F.B., Wang, T., Guo, G.E., 2014. Spatial and temporal distribution of Late Permian–Early Jurassic intrusion assemblages in eastern Qimantag, East Kunlun, and their tectonic settings. Acta Petrol. Sin. 30 (11), 3213–3228 (in Chinese with English abstract).
Wang, H., Feng, C.Y., Li, D.X., Ding, T.Z., Wang, H.Q., Liu, J.N., Zhou, J.H., 2015. Mineralogical characteristics of skarn in Saishitang copper deposit, Xinghai County, Qinghai Province, and their geological significance. Acta Geol. Sin. 36 (3), 313–322 (in Chinese with English abstract).
Wei, G., Zhang, P.B., Li, H.L., Zhang, Z.X., 2012. Characteristics and prospective of the porphyry Cu mineralization in the Saishitang Cu deposit, Xinghai, Qinghai, China. Bull. Mineral. Petrol. Geochem. 31 (5), 510–515 (in Chinese with English abstract).
Whalen, J.B., Currie, K.L., Chappell, B.W., 1987. A-type granites: geochemical characteristics, discrimination and petrogenesis. Contrib. Mineral. Petrol. 95, 407–419.
Wu, T.X., 2010. Geological characteristics and metallogenic model of Saishitang copper deposit in Qinghai Province. Miner. Explor. 1 (2), 140–144 (in Chinese with English abstract).
Wu, F.Y., Yang, Y.H., Xie, L.W., Yang, J.H., Xu, P., 2006. Hf isotopic compositions of the standard zircons and baddeleyites used in U/Pb geochronology. Chem. Geol. 234, 105–126.
Xia, R., Qing, M., Wang, C.M., Li, W.L., 2014a. The genesis of the ore-bearing porphyry of the Tuoketuo porphyry Cu–Au (Mo) deposit in the East Kunlun, Qinghai Province: constraints from zircon U–Pb geochronological and geochemistry. J. Jilin Univ. (Earth Sci. Ed.) 44 (5), 1502–1524 (in Chinese with English abstract).
Xia, R., Wang, C.M., Deng, J., Carranza, E.J.M., Li, W.L., Qing, M., 2014b. Crustal thickening prior to 220 Ma in the East Kunlun Orogenic Belt: insights from the Late Triassic granitoids in the Xiao–Nuomuhong pluton. J. Asian Earth Sci. 93, 193–210.
Xia, R., Wang, C.M., Qing, M., Deng, J., Carranza, E.J.M., Li, W.L., Guo, X.D., Ge, L.S., Yu, W.Q., 2015. Molybdenite Re–Os, zircon U–Pb dating and Hf isotopic analysis of the Shuangqing Fe–Pb–Zn–Cu skarn deposit, East Kunlun Mountains, Qinghai Province, China. Ore Geol. Rev. 66, 114–131.
Xie, L.W., Zhang, Y.B., Zhang, H.H., Sun, J.F., Wu, F.Y., 2008. In situ simultaneous determination of trace elements, U–Pb and Lu–Hf isotopes in zircon and baddeleyite. Chin. Sci. Bull. 53, 1565–1573.
Xin, T.G., Chen, X.Y., Zhu, X.Y., Ding, T.Z., Wang, Y.L., He, P., 2013. Study on the ore genesis of Saishitang skarn copper deposit, Qinghai Province. J. Miner. Explor. 4 (3), 257–265 (in Chinese with English abstract).
Yan, Z., Bian, Q.T., Oleg, A.K., Igor, I.P., Li, J.L., Wang, Z.Q., 2008. Provenance of Early Triassic Hongshuichuan Formation in the southern margin of the East Kunlun Mountains: constrains from detrital framework, heavy mineral analysis and geochemistry. Acta Petrol. Sin. 24 (5), 1068–1078 (in Chinese with English abstract).
Yan, Z., Guo, X.Q., Fu, C.L., Wang, T., Wang, Z.Q., Li, J.L., 2012. Petrology, geochemistry and SHRIMP U–Pb dating of zircons from Late Triassic OIB-basalt in the conjunction of the Qinling–Qilian–Kunlun orogens. Earth Sci. Front. 19 (5), 164–176 (in Chinese with English abstract).
Yang, J.S., Robinson, P.T., Jiang, C.F., Xu, Z.Q., 1996. Ophiolites of the Kunlun Mountains, China and their tectonic implications. Tectonophysics 258, 215–231.
Yang, J.S., Wang, X.B., Shi, R.D., Xu, Z.Q., Wu, C.L., 2004. The Dur'ngoi ophiolite in East Kunlun, northern Qinghai–Tibet Plateau: a fragment of Paleo-Tethyan oceanic crust. Geol. China 31, 225–239 (in Chinese with English abstract).
Yin, A., Harrison, T.M., 2000. Geologic evolution of the Himalayan–Tibetan Orogen. Annu. Rev. Earth Planet. Sci. 28, 211–280.
Yin, H.F., Zhang, K.X., Feng, Q.L., 2004. The archipelagic ocean system of the eastern Eurasian Tethys. Acta Geol. Sin. 78 (1), 230–236.
Yue, Y.G., 2014. Sedimentary Characteristics of Triassic in Southern of the East Kunlun and the Constraints on the Closing Time of A'nimaqing Ocean (Master Degree Thesis), Northwest University, Xi'an, pp. 1–57 (in Chinese with English abstract).
Zhang, Z.Y., 2008. The Formation and Evolution of Paleo-Tethys Small Oceanic of Xinghai in Junction Part of Kunlun and Qinling Orogenic Belts (Doctor Degree Thesis), China University of Geosciences, Wuhan, pp. 1–90 (in Chinese with English abstract).
Zhang, K.X., Lin, Q.X., Zhu, Y.H., Yin, H.F., Luo, M.S., Chen, N.S., Wang, G.C., 2004a. New paleontological evidence on time determination of the east part of the eastern Kunlun mélange and its tectonic significance. Sci. China Ser. D Earth Sci. 47 (10), 865–873.
Zhang, Z.Y., Yin, H.F., Wang, B.Z., Wang, J., Zhang, K.X., 2004b. Presence and evidence of Kuha-i Saishitang Branching Ocean in copulae between Kunlun–Qinling Mountains. Earth Sci. J. China Univ. Geosci. 29 (6), 691–696 (in Chinese with English abstract).
Zhang, H.F., Chen, Y.L., Xu, W.C., Liu, R., Yuan, H.L., Liu, X.M., 2006. Granitoids around Gonghe basin in Qinghai Province: petrogenesis and tectonic implications. Acta Petrol. Sin. 22 (12), 2910–2922 (in Chinese with English abstract).
Zhang, Z.J., Klemperer, S., Bai, Z.M., Chen, Y., Teng, J.W., 2011. Crustal structure of the Paleozoic Kunlun orogeny from an active-source seismic profile between Moba and Guide in East Tibet, China. Gondwana Res. 19, 994–1007.
Zhang, J.Y., Ma, C.Q., Xiong, F.H., Liu, B., 2012. Petrogenesis and tectonic significance of the Late Permian–Middle Triassic calc-alkaline granites in the Balong region, eastern Kunlun Orogen, China. Geol. Mag. 149, 892–908.
Zhang, K.X., Feng, Q.L., Song, B.W., Zhang, Z.Y., Wang, Y.H., Pan, G.T., Lu, S.N., Zhao, X.M., Xing, G.F., 2014a. Non-Smithian strata in the orogen. Earth Sci. Front. 21 (2), 36–47 (in Chinese with English abstract).
Zhang, Z.Y., Ding, T.Z., He, P., Zhu, X.Y., 2014b. Characteristics of superposed folds and its tectonic significance in Saishitang ore district, Qinghai Province—tectonic study on a superposed fold zone. Northwest. Geol. 47 (2), 1–10 (in Chinese with English abstract).
Zhou, T.F., Wang, S.W., Fan, Y., Yuan, F., Zhang, D.Y., White, N.C., 2015. A review of the intracontinental porphyry deposits in the Middle–Lower Yangtze River Valley metallogenic belt, Eastern China. Ore Geol. Rev. 65, 433–456.
Zhu, J.J., Hu, R.Z., Richards, J.P., Bi, X.W., Zhang, H., 2015. Genesis and magmatic–hydrothermal evolution of the Yangla skarn Cu deposit, southwest China. Econ. Geol. 110, 631–652.